Journal of Science: Advanced Materials and Devices 10 (2025) 101034

Contents lists available at ScienceDirect

Journal of Science: Advanced Materials and Devices

journal homepage: www.elsevier.com/locate/jsamd

Review Article

Progress in synthesis of $Ti_3C_2T_x$ MXene-based nanostructures for energy harvesting and storage: A review

Naveen Kumar [a,1], Quy-Van Hoang [b,1], Mohamed Ahmed Belal [c], Kushal Ruthvik Kaja [d], Phi Hung Nguyen [e], Quynh Le-Van [b], Vien Vo [e], Vo Thi Thuy Linh [f], Phan Khanh Thinh Nguyen [g,*], Qui Thanh Hoai Ta [h,**]

[a] Division of Energy & Environmental Technology, Daegu-Gyeongbuk Institute of Science and Technology (DGIST), Daegu, 42988, Republic of Korea
[b] Center for Environmental Intelligence, College of Engineering and Computer Science, VinUniversity, Gia Lam district, Hanoi, 14000, Viet Nam
[c] Graphene Center of Excellence, Energy and Electronics Applications, Egypt-Japan University of Science and Technology, New Borg El-Arab, 21934, Egypt
[d] Department of Physics, Vellore Institute of Technology, Vijayawada, 522237, India
[e] Faculty of Natural Sciences, Quy Nhon University, 170 An Duong Vuong, Gia Lai, Viet Nam
[f] Faculty of Natural Science Education, Pham Van Dong University, Quang Ngai, Viet Nam
[g] School of Chemical, Biological, and Battery Engineering, Gachon University, 1342 Seongnamdaero, Sujeong-gu, Seongnam-si, Gyeonggi-do, 13120, Republic of Korea
[h] Institute of Advanced Technology, Vietnam Academy of Science and Technology, 1B TL29 Street, An Phu Dong Ward, Ho Chi Minh City, Viet Nam

ARTICLE INFO

Keywords:
$Ti_3C_2T_x$ MXene
Synthesis
Properties
Perovskite solar cells
Silicon solar cells and dye-sensitized solar cells
Triboelectric nanogenerators
Supercapacitors and batteries
Printed systems

ABSTRACT

$Ti_3C_2T_x$ MXene, a two-dimensional transition metal carbide, has emerged as a highly promising material for energy harvesting applications due to its exceptional electrical conductivity, large surface area, and tunable surface chemistry. This review presents a comprehensive overview of recent progress in synthesizing $Ti_3C_2T_x$ MXene and its nanostructured composites, highlighting both conventional and fluoride-free etching methods. We explore the integration of MXene with other functional materials to enhance its performance in solar cells, triboelectric nanogenerators, supercapacitors, and printed batteries. Special attention is given to the role of surface terminations, interlayer interactions, and structural modifications in optimizing electrochemical and mechanical properties. Finally, we discuss current challenges-such as oxidation stability, scalable production, and surface functionalization- and propose future directions for advancing MXene-based technologies in sustainable energy systems.

1. Introduction

In modern life, people heavily rely on electronic devices, wearable technology, and it is difficult to imagine a world without these tools, as they offer important convenience and have become essential portable items. Given the rising energy demands associated with wearable devices and the diminishing availability of fossil fuels, there is an urgent necessity for sustainable and viable energy alternatives, as well as green energy resources [1–4]. In recent years, to mitigate environmental pollution and address energy storage challenges, scientists have been studying renewable energy sources such as wind, tidal, solar, geothermal, and hydroelectric power [5–8]. These green energy sources need to be efficiently stored in devices like lithium-ion batteries and supercapacitors. Recent research endeavors have primarily concentrated on two-dimensional materials, attributed to their distinctive properties such as superior optical, electrical, and mechanical characteristics [9–11]. These attributes render them particularly advantageous for a wide range of applications. Among 2D materials, MXene has demonstrated outstanding research potential and holds vast promise for energy harvesting and conversion applications [12–17].

In 2011, Yury's group was the first to explore a new class of 2D materials, including transition metal carbides and carbonitrides/

* Corresponding author.
** Corresponding author.
E-mail addresses: naveen110892@gmail.com (N. Kumar), quy.hv@vinuni.edu.vn (Q.-V. Hoang), mohamedbelal@alexu.edu.eg (M.A. Belal), ruthvikkushalk@gmail.com (K.R. Kaja), nguyenphihung@qnu.edu.vn (P.H. Nguyen), quynh.lv@vinuni.edu.vn (Q. Le-Van), vovien@qnu.edu.vn (V. Vo), vttlinh@pdu.edu.vn (V.T.T. Linh), thinhnpk@gachon.ac.kr (P.K.T. Nguyen), tathanhhoaiqui2292@gmail.com (Q.T. Hoai Ta).
[1] These authors contributed equally to this work.

https://doi.org/10.1016/j.jsamd.2025.101034
Received 17 September 2025; Received in revised form 18 October 2025; Accepted 28 October 2025
Available online 29 October 2025

nitrides, which displayed a combination of naturally hydrophilic surfaces and metallic conductivity. This new emerging family of materials was named MXenes. Their formula is described by $M_{n+1}X_nT_x$ (n = 1–4), where M represents transition metals (Mo, Ta, Sc, Ti, Zr, V, Hf, Cr), X represents carbon and nitrogen, and T_x accounts for functional groups (-F, -OH, -O). $Ti_3C_2T_x$ was the first MXene prepared, which is systematically synthesized by HF etching to remove the Al layers from the Ti_3AlC_2 MAX phase [18–32].

To date, the scientific community has prepared more than 59 different pure MAX phases. The well-known Ti_3AlC_2 MAX precursor has $P6_3/mmc$ symmetry with hexagonal layers that are closely packed into octahedral sites. Generally, the anisotropic Ti-C bond exhibits strong mixed covalent and/or ionic/metallic properties, while the Ti-Al bond exhibits metallic behavior. The bond strength of titanium-carbon bonds exceeds that of titanium-aluminum bonds, allowing chemical agents to selectively remove the Al layers without destroying or interrupting the Ti-C bonds [33–36].

$Ti_3C_2T_x$ MXene possesses a large surface area, excellent electrical conductivity, and low diffusion barriers, which facilitate its use as an electrode material in lithium-ion batteries and supercapacitors. For instance, additive-free MXenes have exhibited volumetric capacitances of up to 1500 F per cubic centimeter (F cm^{-3}), whereas carbon-based composites have shown volumetric capacitances of up to 300 F cm^{-3}, and hydrated ruthenium oxide has achieved capacitances ranging from 1000 to 1500 F cm^{-3} [37]. $Ti_3C_2T_x$ MXene has demonstrated excellent cycling stability when lithium ions intercalate between each layer, in contrast to graphite structures that suffer from severe structural collapse and low cycling rates. Moreover, Ti_3AlC_2 is the most commonly and commercially available MAX phase on the market. Considering all these factors, the functionalization of $Ti_3C_2T_x$ MXene beyond graphene has made it a potential candidate for lithium-ion batteries [38–41]. Another study revealed the size dependence of $Ti_3C_2T_x$ nanosheets through sonication and investigated their electrochemical applications. Using ultrasound methods was shown to significantly improve the etching of MAX phase and greatly increase the electrochemical activity of electrode materials. Therefore, downsizing $Ti_3C_2T_x$ MXene can lead to a remarkable difference in applications, ion conductivity, and surface termination groups [42–46].

Over the past decade, numerous reviews and research have focused on the progress and applications of MXenes in areas such as gas sensors [47,48], batteries [49], supercapacitors [50], water splitting [51], wastewater treatment [52], and biomedical technologies [53]. Most of the review works discuss the fundamental properties and specific applications of MXenes; however, only a few have provided a comprehensive overview of their multifunctional capabilities. Given the rapidly increasing number of publications on MXene-based systems (Fig. 1), a more timely and integrative review is needed. Although several reviews have summarized the properties and applications of MXenes [54,55], there remains a gap in the literature concerning recent advancements in their use for energy harvesting (photovoltaics and triboelectric nanogenerators) and energy storage (supercapacitors and batteries), as well as for water splitting and CO_2 reduction.

In this review, $Ti_3C_2T_x$ MXene is selected as a representative member of the two-dimensional MXene family to highlight its contemporary progress in energy storage and harvesting applications. We begin by discussing the preparation of $Ti_3C_2T_x$ MXene, with a comparison between conventional and fluoride-free etching methods, emphasizing their respective advantages, limitations, and scalability. This is followed by an overview of its physicochemical properties, oxidation behavior, and antioxidant stabilization strategies. Subsequently, the role of $Ti_3C_2T_x$ MXene as a high-performance electrode material is examined across various applications, including solar cells, triboelectric nanogenerators, supercapacitors, printed batteries, photocatalysis, and electrocatalysis. Finally, we present future perspectives on the scalable production of MXenes and their integration into pilot-scale systems and into practical renewable energy technologies.

2. Synthesize methods of $Ti_3C_2T_x$

2.1. Direct HF and in-situ HF etching

HF was employed as the primary etchant for manufacturing MXene from the MAX phase [56,57]. It is demonstrated that the high reactivity between the Al layer and F ion allowed the use of 50 wt% HF to effectively eliminate the aluminum layer from the Ti_3AlC_2 MAX. This process yields accordion-like MXene structures that are maintained through *van der Waals* interactions [58,59]. First-principles calculations were utilized to recognize the mechanism of HF etching. In comparison, different HF concentrations were applied to prepare $Ti_3C_2T_x$, revealing that both HF concentration and etching time suggestively affect the quality of the resulting $Ti_3C_2T_x$ MXene [60–62]. It required 5 h of etching time when using HF concentrations of 30 wt% or higher, whereas only 2 h were

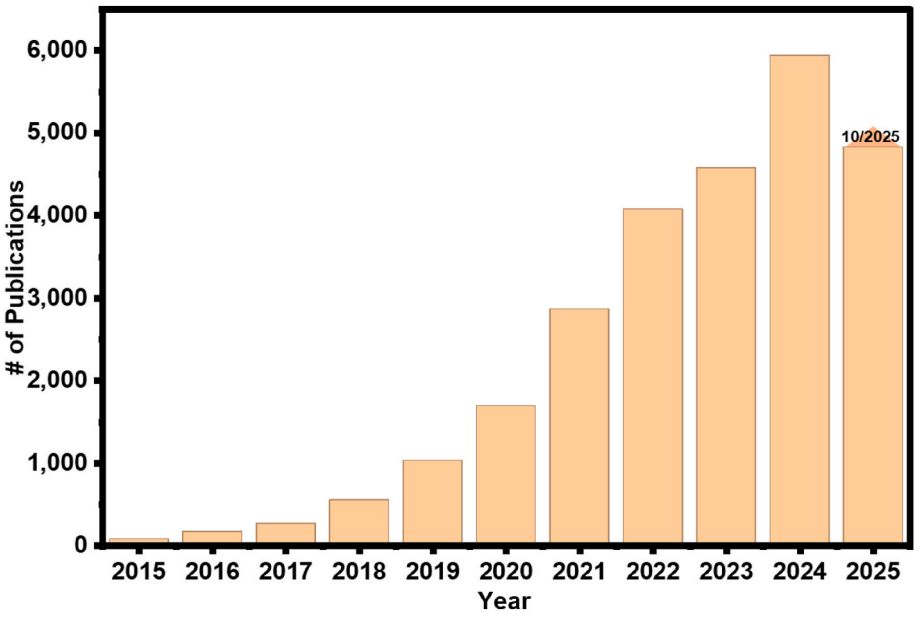

Fig. 1. Publication trend of MXene-related research from Web of Science (2015–2025/10).

sufficient with 50 wt% HF [63]. The sophisticated etching procedure can be explained by the following reactions:

$$Ti_3AlC_2 + 3HF \rightarrow AlF_3 + 1.5H_2 + Ti_3C_2 \quad (1)$$

$$Ti_3C_2 + 2HF \rightarrow Ti_3C_2F_2 + H_2 \quad (2)$$

$$Ti_3C_2 + 2H_2O \rightarrow Ti_3C_2(O/OH)_2 + H_2 \quad (3)$$

$$Ti_3C_2 + 2HF \rightarrow Ti_3C_2F_2 + H_2 \quad (4)$$

HF is a toxic acid with strong corrosiveness, posing risks during the synthesis procedure. Therefore, it is crucial to find alternative etchants to obtain $Ti_3C_2T_x$. HCl and LiF were employed to generate HF *in situ*, providing a safer synthesis approach for $Ti_3C_2T_x$. Various fluoride salts, such as NH_4F, KF, and NaF, have also been used as etchants. As shown in Fig. 2, the Ti_3AlC_2 MAX phase is etched into small slices that are clearly separated from each other. Thus, the use of fluoride-containing etchants was enhanced and supplemented for improved synthesis (see Fig. 3).

2.2. F-free etching

Although conventional $Ti_3C_2T_x$ MXene synthesis typically relies on toxic HF or *in situ* HF etchants, recent advancements have demonstrated the successful preparation of F-free MXenes, which offer improved safety, controllable surface terminations, and enhanced tunability. For example, Youbing and co-workers synthesized Cl-terminated MXene using a Lewis acidic etching approach. In this process, a mixture of Ti_3SiC_2 MAX and $CuCl_2$ was heat-treated at 750 °C. During the reaction, Si atoms tended to oxidize into Si^{4+} cations due to the weak Ti–Si bonding, subsequently reacting with Lewis acidic Cu^{2+} to form volatile $SiCl_4$ and metallic Cu. After etching, ammonium persulfate was employed to remove by-products such as Cu particles, $SiCl_4$, and residual $CuCl_2$ [65]. Ali et al. synthesized Br-terminated MXene under glovebox conditions at room temperature. Specifically, a mixture of Ti_3AlC_2 and bromine in a 1:8 M ratio was stirred in cyclohexane for 8 h. The resulting supernatant was collected and subsequently washed with tetrabutylammonium bromide and organic solvents such as tetrahydrofuran. Interestingly, the surface termination groups can be further tailored by employing different halogen sources during the etching process, including iodine, iodine monobromide, and iodine monochloride [66].

It has been confirmed that the alkali-assisted hydrothermal technique can prepare F-free $Ti_3C_2T_x$ MXenes without any hazardous issues. Li et al. demonstrated a NaOH-assisted hydrothermal technique to synthesize $Ti_3C_2T_x$ MXene with T_x = -O, -OH at 270 °C [67]. There are two steps to remove Al layers: first, Al oxidation to AlO_2 and then its dissolution in alkali. Deprived of the F groups, the $Ti_3C_2T_x$ film electrode displayed excellent supercapacitor performance (314 F g^{-1} in H_2SO_4), that is better than $Ti_3C_2T_x$ MXene synthesized using HF etching. In a similar scenario, Yang et al. confirmed an efficient F-free etching technique for the preparation of MXene using anodic corrosion of Ti_3AlC_2 MAX phase in binary aqueous electrolyte [68]. The dissolution of the A

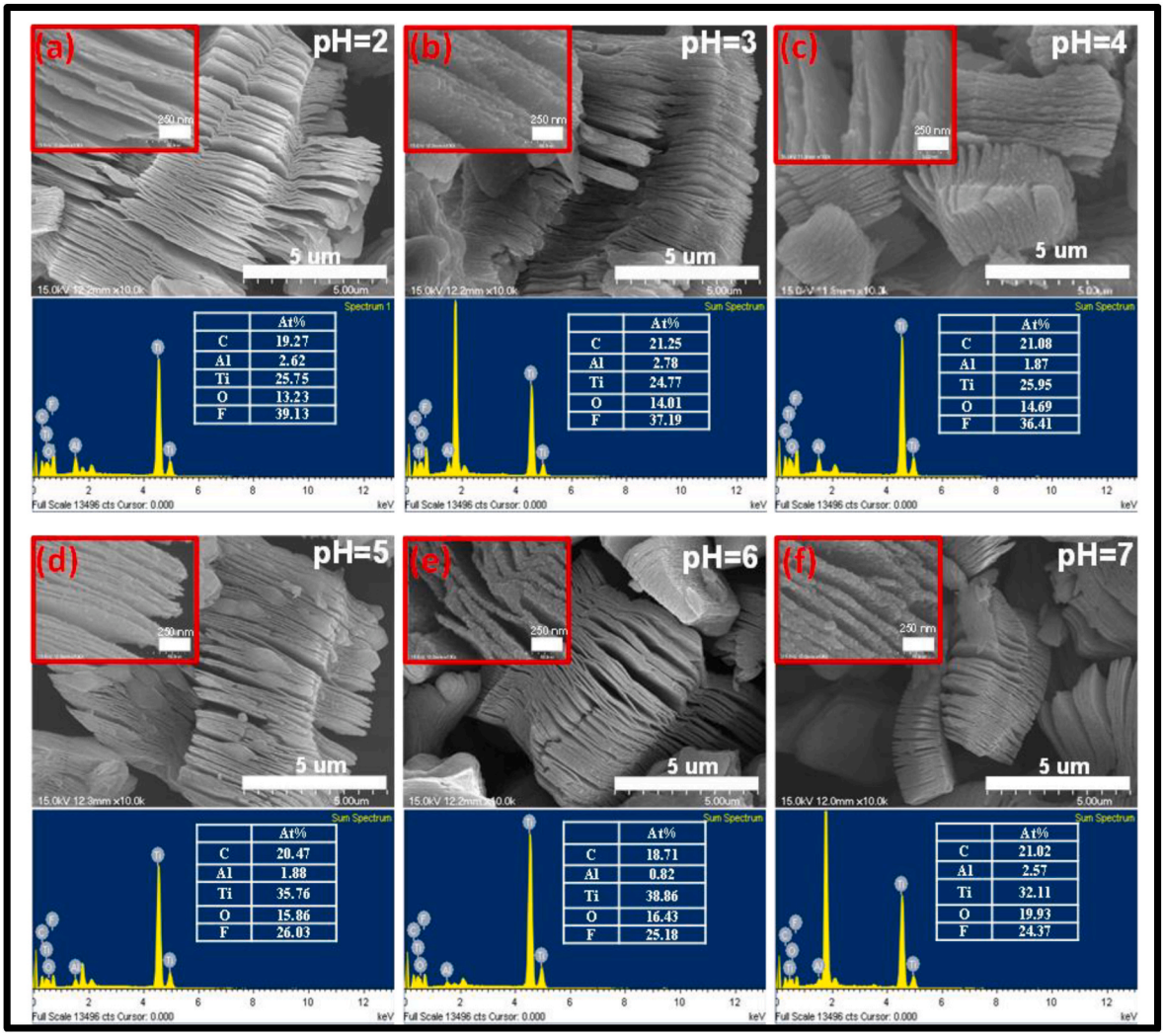

Fig. 2. SEM image of $Ti_3C_2T_x$ MXene at different pH value. Reprinted and adapted with permission from Ref. [64].

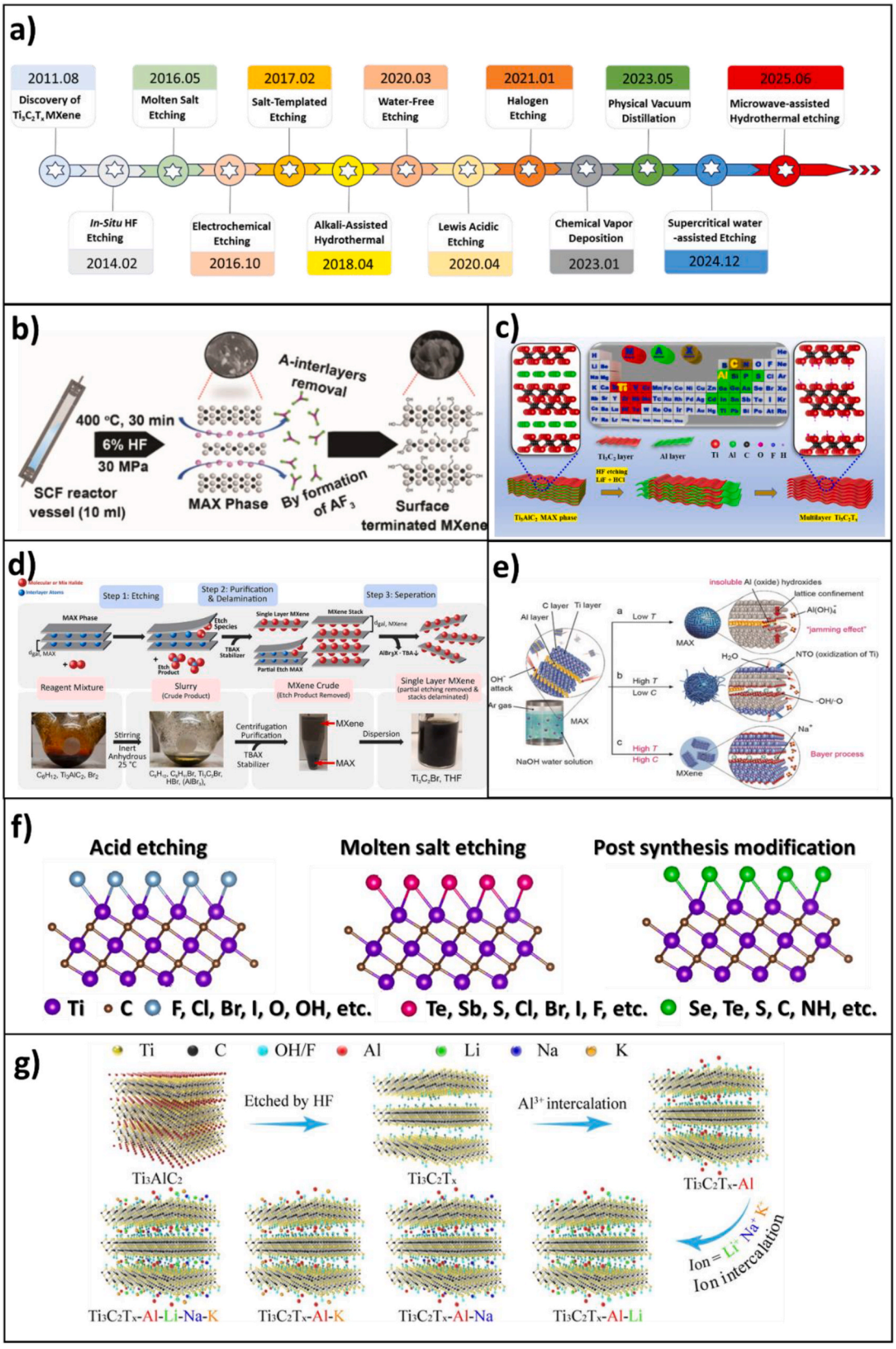

Fig. 3. a) Timeline of the development and evolution of MXene synthesis methods since 2011. MXene synthesis has been achieved through various approaches, including: b) Supercritical water-assisted etching. Reprinted and adapted with permission from Ref. [71]. c) HF or HCl/LiF etching. Reprinted and adapted with permission from Ref. [72]. d) Halogen etching. Reprinted and adapted with permission from Ref. [66]. e) Alkali treatment. Reprinted and adapted with permission from Ref. [73]. f) Surface functional group modification. g) Ion pre-intercalation of MXene. Reprinted and adapted with permission from Ref. [69].

layer, succeeded by *in-situ* intercalation of NH_4OH, led to the successful extraction of $Ti_3C_2T_x$ MXene with a notable yield of 90 % and an approximate size of 19 μm. Moreover, the intercalation of K^+, Li^+, and Na^+ ions enable $Ti_3C_2T_x$ MXene to retain its accordion-like morphology with a densely stacked hexagonal crystal structure. Ion intercalation not only enriches the surface functional groups but also increases the interlayer spacing at the atomic scale, thereby enhancing electrochemical performance through the columnar effect within the interlayer voids of $Ti_3C_2T_x$ MXene [69,70].

As summarized in Table 1, the synthesis of $Ti_3C_2T_x$ MXene is strongly influenced by multiple parameters, including the selection of etching agents, concentration, reaction time, and the nature of surface terminations. Each application demands a tailored synthesis route; for example, HF-based etching offers high yield, excellent conductivity, and well-developed reproducibility, making it suitable for energy conversion systems. However, the use of toxic and corrosive HF introduces serious safety risks, waste management challenges, and environmental burdens, which substantially hinder industrial scalability. In comparison, the LiF/HCl-assisted *in situ* HF method provides better delamination efficiency and fewer structural defects, offering improved dispersibility for electronic or sensor applications, but still suffers from fluoride contamination and limited oxidation stability.

To address these drawbacks, fluoride-free etching strategies; such as Lewis-acidic molten salts, halogen-mediated, or electrochemical etching, have recently emerged as safer and more environmentally benign alternatives, enabling tunable surface terminations and potentially improved oxidation resistance. Nevertheless, these approaches often require high-temperature processing (600–800 °C), complex purification steps, and lower delamination yields, which currently restrict their large-scale implementation. Therefore, future studies should prioritize the design of additive-free, low-temperature, and scalable synthesis routes capable of delivering defect-controlled, few-layer $Ti_3C_2T_x$ MXene nanosheets with consistent quality, thereby bridging the gap between laboratory synthesis and industrial production.

Table 1
Comparison between conventional fluoride-based and fluoride-free etching strategies for $Ti_3C_2T_x$ MXene synthesis.

Category	Fluoride-based etching (HF or *in situ* HF)	Fluoride-free etching (Lewis acidic, electrochemical, alkali, or halogen-based)
Typical reagents	HF (40–50 %), LiF + HCl (*in situ* HF)	$CuCl_2$, $ZnCl_2$, Br_2, I_2, ICl, IBr, NaOH, H_2SO_4, electrochemical electrolytes
Reaction temperature	Room temperature to ~60 °C	25–800 °C (depending on method; e.g., 600–800 °C for molten salts)
Reaction duration	12–72 h (depends on MAX phase)	Minutes to several hours (molten salt), or 1–6 h (electrochemical)
Delamination yield	High (up to 80–90 % few-layer dispersions)	Moderate (30–60 %), often requires post-intercalation and ultrasonication
Surface terminations	–F, –O, –OH	–Cl, –Br, –I, –O (tunable depending on halogen source)
d-spacing	8 -11 Å	12 -14 Å
Electrical conductivity	Typically high ($>10^3$–10^4 S cm^{-1})	Comparable or slightly lower (Depends on termination and defects)
Oxidation stability	Moderate; F-terminations may promote oxidation in aqueous media	Potentially higher (Cl-terminated MXenes show improved resistance)
Advantages	Mature, reproducible process Low energy input High delamination yield Compatible with Li^+ intercalation	HF-free (safe and eco-friendly) Controllable surface chemistry Expanded range of terminations Reduced fluorine contamination
Limitations	Toxic and corrosive reagents Hazardous waste management F-terminations may block active sites Oxidation susceptibility	Higher temperature and energy demand Complex purification Lower delamination yield Inconsistent flake quality
Environmental and safety aspects	Requires strict safety handling and HF-resistant equipment	Safer operation; reduced hazardous effluents
Scalability	Feasible at lab scale; costly at industrial scale due to HF containment	Promising for pilot scale; electrochemical methods most scalable

3. Properties of $Ti_3C_2T_x$

A fundamental understanding of surface interactions and properties is a prerequisite for modulating MXene for potential applications. According to DFT, $Ti_3C_2T_x$ is characterized by six-fold symmetry, a hexagonal lattice structure with a coordination number of 6, and a rhombic lattice configuration when viewed from above [74]. The single carbon layer is located between two titanium layers. Along with pure $Ti_3C_2T_x$ MXene, their properties are influenced by functional groups. For example, Wang and co-workers confirmed that the functional groups are randomly covered and distributed over the $Ti_3C_2T_x$ surface rather than forming a specific domain, with -OH and -F directly bonded to the surface of $Ti_3C_2T_x$ MXene [75].

Hydrogen bonding interactions and *van der Waals* forces are present between each layer and the associated functional groups. The strength of the hydrogen bonding is influenced by the spatial arrangement and orientation of hydroxyl groups on one surface in relation to the -O and -F groups on the opposing surface [75].

The type of functional groups depends on the method and concentration of HF used. For instance, $Ti_3C_2T_x$ synthesized using HCl-LiF etching will have more -O groups and fewer -F groups compared to $Ti_3C_2T_x$ synthesized with 50 % HF. According to DFT calculations, the orientation of T_x is energetically favorable when T_x groups are located on top of carbon atoms and/or in hollow spaces, as shown in Fig. 4 [76]. Therefore, the most stable configurations are $Ti_3C_2(O)_2 > Ti_3C_2(OH)_2 > Ti_3C_2F_2$ due to steric hindrance between surface terminations and carbon atoms [76]. Moreover, $Ti_3C_2T_x$ MXene easily oxidizes under ambient conditions. Xie et al. reported that $Ti_3C_2(O)_2$ MXene is more stable than $Ti_3C_2(OH)_2$ and $Ti_3C_2F_2$ because -OH and -O tend to replace -F under ambient conditions and at high temperatures [77].

Lipatov and co-workers confirmed the highest Young's modulus (0.33 ± 0.03 TPa) for a $Ti_3C_2T_x$ single layer using AFM nanoindentation measurements [79]. The MXene thin films, approximately 20 nm in thickness, synthesized utilizing an NH_4HF_2 solution, demonstrated a transmittance of 90 % across the visible to infrared spectrum. In another work, the calculated Young's modulus and fracture strength of single-layer $Ti_3C_2T_x$ MXene measured using a push-to-pull device were approximately 484 GPa and 16 GPa, respectively, which are consistent with the values predicted by molecular dynamics simulations (Fig. 5(a, b)). These values are higher than those of $MoSe_2$ and comparable to those of graphene, suggesting that $Ti_3C_2T_x$ MXene is a promising alternative to carbon-based materials for strain engineering applications due to its intrinsic mechanical properties and brittle fracture behavior [80].

Hantanasirisakul and co-workers investigated a fundamental technique to prepare homogeneous, transparent $Ti_3C_2T_x$ MXene films using spray coating of exfoliated colloidal $Ti_3C_2T_x$ aqueous solutions over various substrates [81]. The transmittance was measured to be around 91.2 % for 5 nm thick films and 43.8 % for 70 nm thick films. There is an inherent trade-off between transmittance and conductivity for thin films. For example, Ali et al. synthesized transparent and thin $Ti_3C_2T_x$ MXene films using an electrohydrodynamic atomization procedure in a vacuum-free environment with an electric field on a glass substrate [82]. They achieved a resistivity of 3.4×10^{-4} Ω/cm with a 135 nm thin film and 87 % transmittance under diode behavior (3V, 120 mA).

In $Ti_3C_2T_x$ MXenes, the intercalation between layers has poor strength, facilitating the insertion of different species such as ionic,

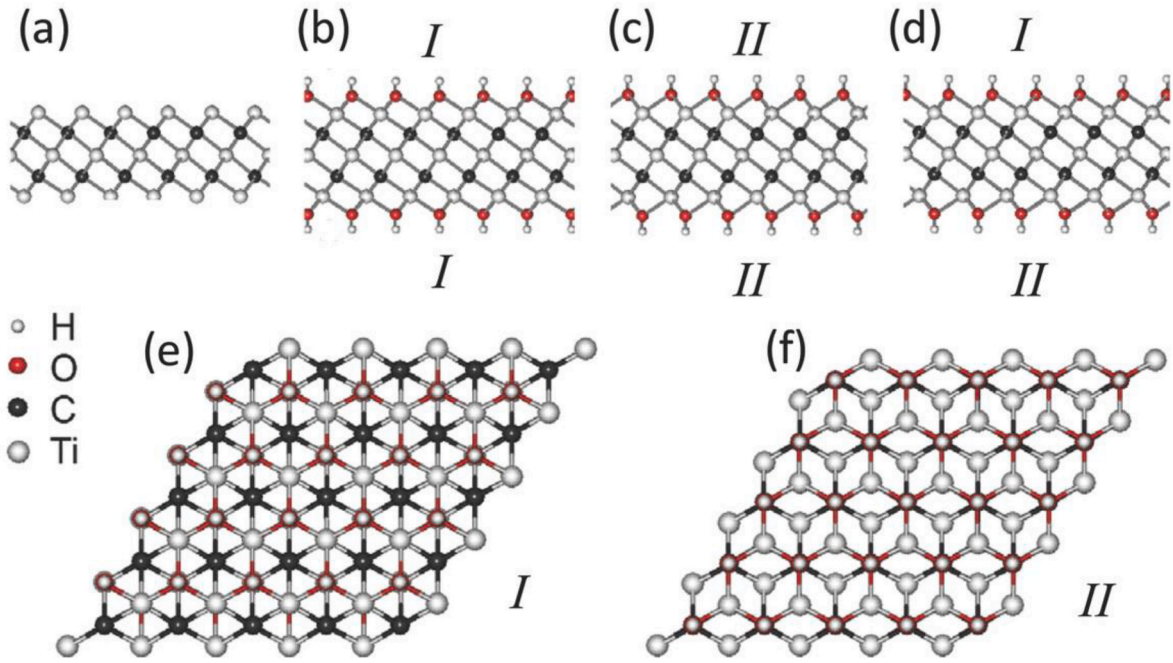

Fig. 4. Atomic structure of MXene. Reprinted and adapted with permission from [78].

organic, and polymeric species. The intercalation of cations is crucial due to its unique chemical behavior and physical properties. For instance, Xiong and co-workers confirmed that the sliding of $Ti_3C_2T_x$ MXene was relatively smoother with intercalated Li^+ cations, which improved the rheological properties [83]. Wang et al. reported that Al ion intercalation facilitated the horizontal sliding of single-layer $Ti_3C_2T_x$ MXene and redefined the MXene structure [84]. Since intercalation chemistry is crucial for energy storage, the Li^+ ion charge storage mechanism in MXenes was confirmed by X-ray absorption spectroscopy measurements, showing that the oxidation state of Ti varied consistently. However, the oxidation state remained stable when the potential was reduced, and a lithium layer was created [85]. As shown in Fig. 5(c), the rheological properties of $Ti_3C_2T_x$ MXene dispersions in water were investigated by Bilen et al. [86]. As a result, a shear-thinning behavior was observed at high MXene loading (70 %) based on viscosity measurements. Unlike other colloidal systems, at low concentrations (1 mg/mL), MXene exhibited an early spike in viscosity owing to its low mass and large surface charge (−46 mV). The elastic component was detected even at very low concentrations (<0.2 mg/mL). In contrast, higher elasticity and viscosity were recorded in samples containing a greater mass of nanostructures, which are suitable for applications requiring a high elastic modulus, such as extrusion printing. Although several studies have investigated the apparent viscosities of $Ti_3C_2T_x$ dispersions [87], further rheological studies are still needed to elucidate the relationship between the shear field, surface functional groups, and particle geometry.

4. Oxidation, storage, and life time

Among the various factors influencing the oxidation behavior of $Ti_3C_2T_x$ MXene, the most critical are the synthetic methods, post-synthetic treatments, and storage environments. Specifically, each etching method induces distinct defects in surface morphology and functional groups. As shown in Fig. 6, the oxidation degradation of MXene generally initiates at atomic defect sites and nucleation points, leading to the formation of amorphous carbon and TiO_2. Owing to the relatively low surface energy (0.44 J/m^2) of the (101) lattice plane compared with the (001) (0.90 J/m^2) and (100) (0.53 J/m^2) planes, the preferential growth of TiO_2 nanostructures on the basal plane of MXene predominantly happens along the (101) orientation [88,89]. Besides, under heat treatment at different temperatures, TiO_2 begins to form on the surface of MXene while the 2D structure is retained below 600 °C [90]. At 350 °C, a cubic TiO_2 phase is formed, accompanied by the removal of surface –OH groups driven by thermal treatment under ambient atmosphere [59]. When the temperature exceeds 800 °C, the accordion-like structure of MXene is completely degraded, resulting in the formation of anatase and rutile TiO_2. Under an Ar inert atmosphere, MXene preserves its 2D morphology even at 1000 °C, whereas TiO_2 nanostructures are observed at 200 °C under an O_2 atmosphere [91]. In an NH_3 environment, nitrogen atoms are doped into the MXene matrix by substituting carbon sites at 700 °C [92]. Moreover, the storage conditions of MXene play a crucial role in preserving its structural integrity and electrical conductivity.

Zhang et al. demonstrated that the storage temperature is linearly correlated with the oxidation rate of MXene [93]. The morphological structure and electrical properties of MXene exhibited slight changes after two days of storage at ambient conditions, whereas the frozen dispersion showed no noticeable alteration. This stability is attributed to the solid ice matrix, which significantly reduces the diffusion rate and contact of oxygen with $Ti_3C_2T_x$ MXene. The freezing method thus provides an effective approach for ultra-long-term storage of MXene, maintaining its electrical, mechanical, and energy storage properties for over 1.5 years without degradation.

Across solid, liquid, and gaseous phases, it has been demonstrated that MXene stored in ice exhibits greater stability and better retention of properties compared to that stored in aqueous solutions, owing to oxidative degradation in water [94,95]. Consequently, $Ti_3C_2T_x$ MXene is preferably stored in organic solvents, particularly ethanol, at low temperatures (below 5 °C) and under basic pH conditions, thereby suppressing electron delocalization at the titanium sites.

Moreover, to address the stability challenges and broaden the application of MXene in diverse environments, several strategies have been developed, including green synthesis and hybridization with polymers or MOFs. For example, Zhang and co-workers fabricated PSS/PEDOT/$Ti_3C_2T_x$ composites for use in flexible electronic devices, achieving an excellent volumetric capacitance of approximately 614.5 F cm^{-3} at a scan rate of 5 mV/s [96]. In this optimized composite, MXene serves as the medium for intersheet charge transport and energy storage,

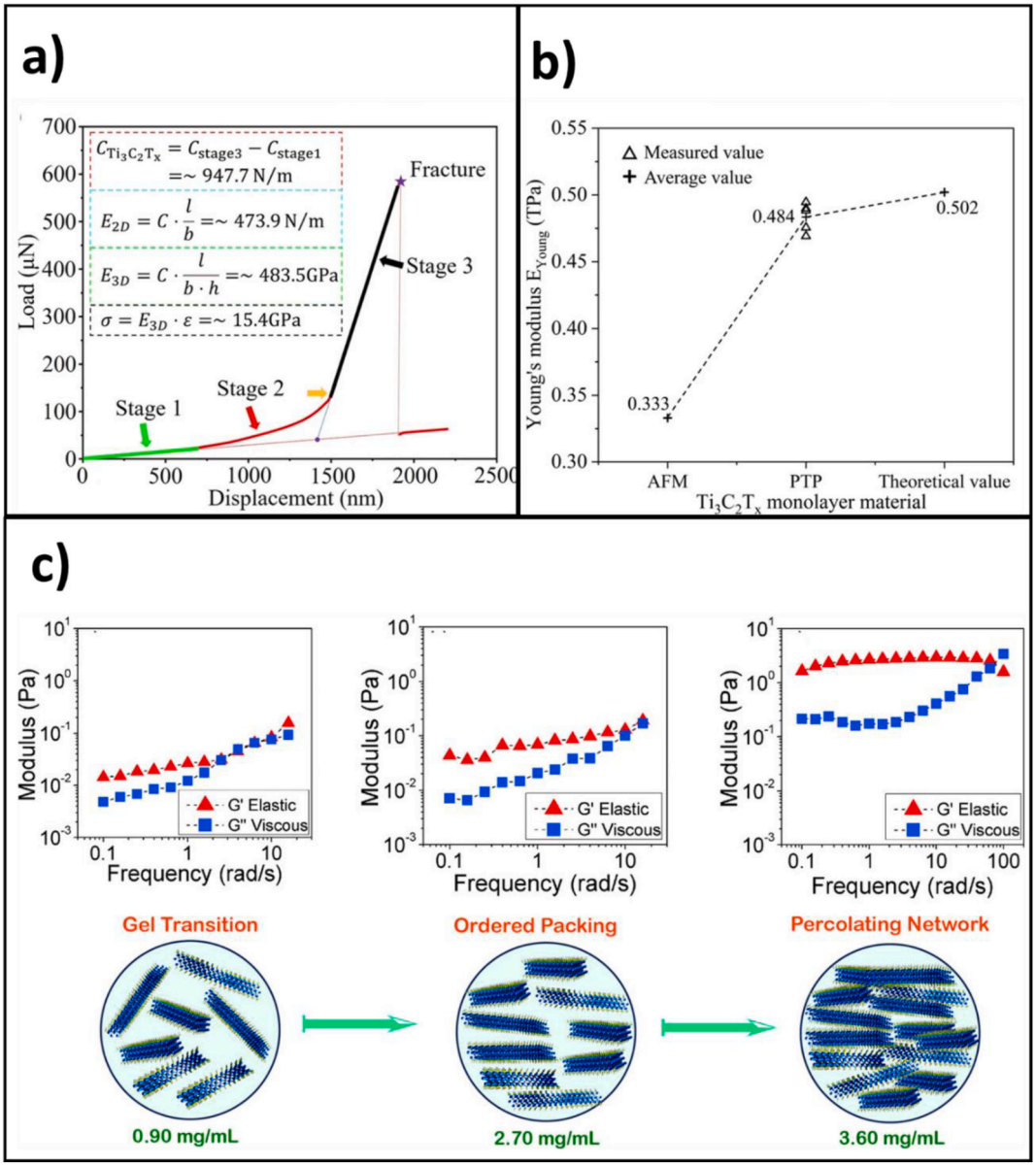

Fig. 5. (a, b) The Tensile strength and Young'modulus of single layer MXene. Reprinted and adapted with permission from Ref. [80]. c) Rheological properties of $Ti_3C_2T_x$ MXene at different concentrations (0.9 mg/mL, 2.7 mg/mL, 3.6 mg/mL). Reprinted and adapted with permission from [86].

while the PEDOT:PSS polymer chains provide mechanical strength and flexibility. Similarly, the green synthesis of $Ti_3C_2T_x$/PEDOT:PSS electrodes has been employed for microsupercapacitor applications [97]. Zn^{2+} ions were introduced during the coagulation process, disrupting electrostatic repulsion and acting as both bridging and protective agents between MXene layers, thereby enhancing the solidification of $Ti_3C_2T_x$/PEDOT:PSS fibers. In another study, MXene was effectively protected through combination with ligands, owing to the hydrophobic characteristics of alkylated 3,4-dihydroxy-L-phenylalanine ligands, which exhibited excellent electrical performance and oxidation stability. After nearly three weeks of operation under 85 % relative humidity, the composite retained approximately 90 % of its initial electrical conductivity, attributed to both π–electron interactions and hydrogen bonding [98]. Furthermore, Tae and co-workers demonstrated that ligand-functionalized $Ti_3C_2T_x$ composites maintained stable performance for up to six weeks when applied as printed electronics in thin-film transistors [99].

Despite these efforts, each method possesses inherent advantages and limitations concerning the oxidation behavior of $Ti_3C_2T_x$ MXene (Table 2). A deeper and more systematic investigation, integrating machine learning and mechanistic modeling, is required to comprehensively elucidate the fundamental oxidation mechanisms, storage stability, and lifetime of MXenes under various processing and environmental conditions, prior to their scale-up and integration into practical technologies [100].

5. Potential application of $Ti_3C_2T_x$

5.1. MXene-based materials for energy harvesting

MXenes, a family of two-dimensional transition metal carbides, nitrides, and carbonitride, have shown to be a good choice for different charge carrier layers in photovoltaic applications due to their tailorable electrical characteristics by compositional and functional group modification [117]. The tunable band gap and electronic conductivity makes it suitable for being used as both ETL and HTL. Apart from having good electrical conductivity and mechanical flexibility, it also shows high hydrophilicity which helps in the good wettability for perovskite and

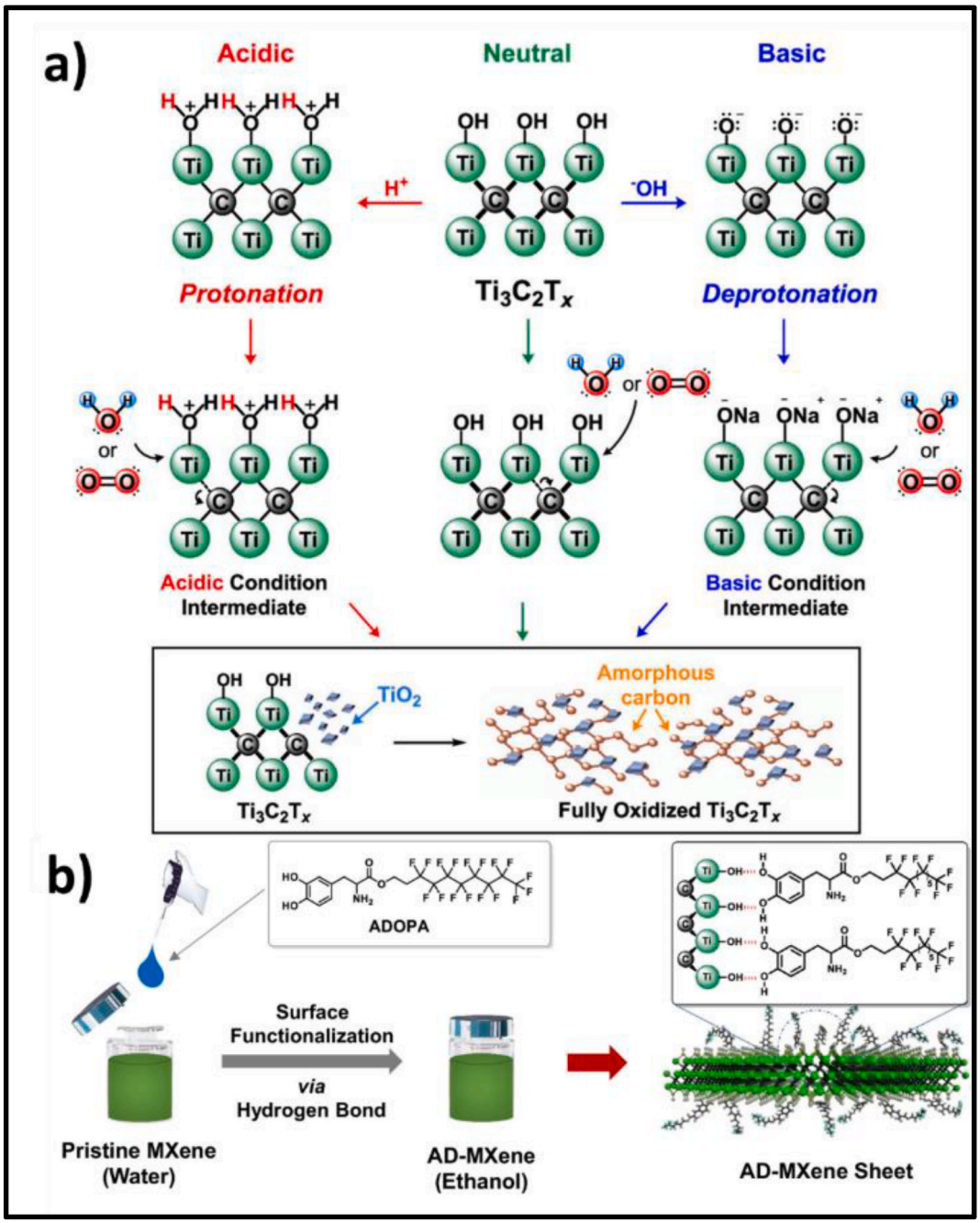

Fig. 6. a) The plausible mechanism of $Ti_3C_2T_x$ oxidation under acidic and basic conditions. Reprinted and adapted with permission from Ref. [101]. b) Schematic illustration of the ligand-functionalization procedure for $Ti_3C_2T_x$ MXene. Reprinted and adapted with permission from [99].

other organic absorber layers for solar cells.

5.1.1. Perovskite solar cells

Over the last decade, perovskites have achieved major advances in photovoltaics and associated sectors. However, hurdles remain in improving their performance and addressing stability concerns to permit future commercialization. The development of a unique 2D halide perovskite material represents a significant advancement in solar energy conversion efficiency. Since its original announcement in 2018, the incorporation of a novel 2D material, MXene, into perovskite solar cells has yielded encouraging results. This material exhibits excellent transparency, electrical conductivity, carrier mobility, extraordinary mechanical strength, and an adjustable work function [117].

Double-layered methyl ammonium (MA)-free Cs_2BiAgI_6 PSCs band gap of 1.6 eV with MXene + TiO_2 as the ETL shows a significant improvement in EQE and PCE of the PSCs [118]. The novel approach of using MXene combined with TiO_2 as an ETL in PSCs significantly improves performance while potentially reducing manufacturing costs and defects. This combination achieved a remarkable PCE of over 28 %, with an V_{OC} of 1.48 V, J_{SC} of 22.8 mA cm^{-2}, and an FF of 84.6 %. (A detailed quantitative summary of these and other representative MXene-engineered PSCs is provided in Table 3, highlighting their respective J–V parameters and stability improvements). Saranin et al. showed that MXenes in NiO based inverted solar cell play a crucial role in passivating trap states within the cell structure, leading to enhanced charge extraction and collection at the electrodes [119]. Their presence also allows for easy tuning of energy level alignment at perovskite/ETL interfaces. As a result, MXene-based engineered cells exhibited

Table 2
Summary of current techniques for enhancing MXene stability.

Specific strategy to improve MXene stability	Advantages	Disadvantages
Collection of purity and quality MAX phase [102,103]	Improves the quality and purity of synthesized MXene at the raw material stage	Possible introduction of impurities
Optimization of etchant type and concentration [104, 105]	Enables optimized preparation with controlled surface termination	Non-uniform surface terminations, low reproducibility.
Production of large-sized nanostructures [106]	Enhances structural stability and electrical properties simultaneously	Restricted application cases
Edge or surface protection [107]	Provides isolation from moisture and oxygen	May affect electrical performance and dispersion
Surface modification [108,109]	Modifies surface chemistry to control oxidation and improve stability	May alter intrinsic electrical properties
Heat treatment [110]	Improves electrical performance	Requires high temperature; limited universality
Construction of Composite-derived MXene [59,111]	Combines MXene with complementary materials to improve stability	Involves complex fabrication processes; not universally applicable
Storage in inert ambient at low-temperature [112]	Simple, universal, and effective for oxidation suppression	High operational cost. Limited practicality for large-scale storage
Freezing storage [93]	Simple and low-cost method to inhibit oxidation	Energy demand for long-term freezing. Possible flake aggregation upon thawing
Storage in organic solvents [112,113]	Provides better inhibition of degradation than aqueous media	Requires MXene separation prior to reuse
Oxide/MOF/Hydrogel encapsulation [114–116]	Effectively isolates MXene from the external environment	Increases fabrication cost and sophisticated fabrication technique

significantly improved performance compared to conventional devices, achieving a power PCE of over 19 %. While the average V_{OC} values slightly declined in all structures using MXenes, this decrease was outweighed by a significant increase in JSC, leading to an overall improvement in PCE (This trend is clearly reflected in Table 3, where MXene-based ETLs consistently show current density enhancement despite minor V_{OC} variations). This approach presents new opportunities for the development of inverted PSCs, offering great potential for large-area device integration and long-term stability. Niu et al. demonstrated the use of Nb_2C MXenes as an additive to SnO_2 ETLs to improve the performance and stability of PSCs [120]. The addition of Nb_2C MXenes resulted in larger SnO_2 grain growth, enhanced surface energy, reduced defects, and improved carrier transport, leading to PSCs with a champion efficiency of 22.86 %, a significant increase from the control's 18.96 %. Furthermore, these PSCs showed impressive stability, retaining 98 % of their initial efficiency after 40 days at 25 °C and 40–60 % humidity, compared to just 85 % for the control devices (Table 3).

Yang et al. explored the use of Ti_3C_2 MXene in organic-inorganic lead halide perovskite solar cells to enhance efficiency [121]. By incorporating Ti_3C_2 into the SnO_2 layer, the short-circuit current density (J_{SC}) increased from 22.83 to 23.56 mA/cm^2, with an optimal Ti_3C_2 concentration of 1.0 wt% yielding a PCE above 18 %. The improved electron transport pathways facilitated better charge collection, though excessive Ti_3C_2 loading reduced V_{OC} and *FF*, leading to lower PCE. Devices with pure Ti_3C_2 as the ETL showed poor efficiency (5.28 %), confirming the necessity of a composite ETL structure.

Zhang et al. investigated the role of the HTL in PSCs, emphasizing its impact on both hole transfer efficiency at the perovskite/HTL interface and the crystallization process of the perovskite film [122]. In their study, Nb_2CT_x MXene was synthesized and utilized as the HTL due to its outstanding photoelectric properties. To optimize its W_F, oxygen plasma treatment was applied to enhance the –O terminated functional groups on the Nb_2CT_x surface, thereby improving its effectiveness in inverted PSCs.

(i) Improved environmental stability MXene surface termination due to its hydrophilic nature helps in better adhesion on the surface and moisture resistance which is shown to be have retained over 90 % of their initial efficiency after 1000 h of continuous illumination and humidity in exposure to open environmental conditions [123];
(ii) Reduced recombination losses: presence of trap states and defects across the surface of perovskite and at the junction with ETL leads to reduced charge transport and increased recombination losses which are a deterrent to achieving high efficiency. Adding MXenes to the perovskite/ETL interface can dramatically minimize charge recombination. Jin et al. showed a reduction in recombination losses and an increase in efficiency with the use of $Ti_3C_2T_x$ MXene interlayers [124].

5.1.2. *Silicon solar cells and Dye-Sensitized solar cells*

Though a lot of research has been done to find the alternative solution to silicon based solar cells it still remains the most prevalent used commercial solar cell due to its high efficiency and stability. Efforts are still made to further enhance its performance with use of various passivation layers and other strategies. MXene interlayers have also been studying surface passivation and reduced charge recombination velocities. MXene coating on Silicon wafer has helped in increasing its PCE [129]. Apart from passivating layer MXene has shown its potential as antireflective coating like MgF_2 [130], thus resulting in better absorption of photon leading to better photocurrents, hence enhanced power conversion.

Though not used extensible, MXene has potential to be used as a counter electrode due to its superior conductivity which can replace expensive platinum electrodes thus paving way to reduce overall cost of the device. As discussed in the earlier sections also Mxene has high photocatalytic properties reducing Triiodide to iodide essential reaction in DSSCs which improves the overall PCE. A 2D/2D MXene–graphene composite has been developed as an alternative counter electrode for DSSCs, achieving a power conversion efficiency of 6.4 %, comparable to the traditional platinum-based electrode [131].

Table 3
Performance metrics table of representative MXene-based PSCs.

Device (MXene role)	V_{OC} (V)	J_{SC} (mA cm^{-2})	FF (%)	PCE (%)	Stability/notes	Ref.
SnO_2 + $Ti_3C_2T_x$ (1.0 wt‰) — ETL additive	~1.06	~23.14	~75	~18.34 (average)	Retained ≈ 80 % of PCE after >30 days ambient storage	[125]
Pristine $Ti_3C_2T_x$ as ETL (no SnO_2)	~0.93	~13.7	~41	~5.3 (champion)	Poor electron transport — demonstrates need for composite ETL	[125]
Surface-oxidized $Ti_3C_2T_x$ MXene (passivation layer)	1.17	18.81	78.8	17.35 (forward scan)	Excellent stability: >90 % PCE retained after 1000 h under 85 °C/RH 40 %	[126]
Plasma-oxidized $Ti_3C_2T_x$ MXene ETL	0.84	23.27	61.9	12.10 (0 min)	Higher plasma time increased wettability & band alignment	[127]
Nb_2C MXene additive in SnO_2 ETL	1.138	25.29	79.5	22.86 (champion)	Retained 98 % PCE after 40 days (25 °C, 40–60 % RH)	[128]

5.1.3. Triboelectric nanogenerators

TENGs are devices that transform mechanical energy into electrical energy via contact electrification and electrostatic induction [132,133]. They have arisen as a potential device for capturing ambient mechanical energy from several sources, including human motion, wind, and water waves [134,135]. The integration of MXenes into TENGs has led to significant advancements in energy harvesting technology. MXenes enhance TENG performance due to their unique electronic properties, tunable surface chemistry, and excellent mechanical characteristics [136]. Their incorporation results in increased output voltage, current density, and overall energy conversion efficiency [137,138]. The layered structure of MXenes facilitates rapid electron transport, while their surface properties can be optimized to improve triboelectric performance. $Ti_3C_2T_x$ MXene-based TENGs exhibit superior flexibility, durability, and even self-healing capabilities, expanding their potential applications in wearable electronics and harsh environments [139,140]. MXenes can function as both triboelectric materials and conductive electrodes, simplifying device design. Moreover, their ability to significantly improve the dielectric constant and surface charge density of composite materials has led to remarkable improvements in TENG output [141]. Recently Mondal et al. utilized $Ti_3C_2T_x$ nanosheets as a key component to enhance the performance of a TENG. They synthesized MXene by etching the aluminum layer from the MAX phase Ti_3AlC_2 utilizing concentrated HCl, followed by delamination. The MXene sheets were then incorporated into a PVDF matrix to create a nanocomposite for the top layer of a double-layer electronegative structure in the TENG. The bottom layer consisted of PDMS with embedded $NaNbO_3$ nanoparticles. This innovative double-layer design aimed to simultaneously enhance charge generation and improve charge retention in the TENG is shown in Fig. 7(a). The significant electronegative characteristics of MXene in the top PVDF layer enhanced the electron affinity of the friction layer, leading to improved charge generation during contact electrification. Meanwhile, the ferroelectric $NaNbO_3$ nanoparticles incorporated in the lower PDMS layer enhanced internal polarisation and introduced extra trap sites, thereby augmenting the retention of the generated surface charges. The synergistic impact of these two layers significantly improved TENG's performance. The optimized double-layer structure with 15 wt% MXene in PVDF and 15 wt% $NaNbO_3$ in PDMS (15MP/15NP) yielded impressive results, generating a voltage of 150 V and a current of 4.3 μA. The power density achieved was 134 $\mu W/cm^2$, representing an increase of approximately 5.8 times compared to a TENG utilizing a single PVDF electronegative layer, as shown in Fig. 7(b). The fabricated device is utilized for signal transfer in wireless communication [142]. In 2022, Yang et al. used niobium carbide (Nb_2CT_x) MXene as a key component in developing a high-performance TENG. They synthesized Nb_2CT_x nanosheets through a two-step process: first, etching Nb_2AlC MAX phase with LiF/HCl to remove the aluminum layer, then intercalating with tetrabutylammonium hydroxide (TBAOH) to achieve monolayer nanosheets [143]. The innovative aspect of their work lies in creating a hybrid film combining 1D CNT, 2D Nb_2CT_x MXene, and conductive polymer PEDOT using a one-step vacuum-assisted filtration technique. SEM reveals the morphology of Nb_2CT_x MXene having an accordion-like structure shown in Fig. 7(c). In the flexible TENG sensor, this hybrid film functioned as

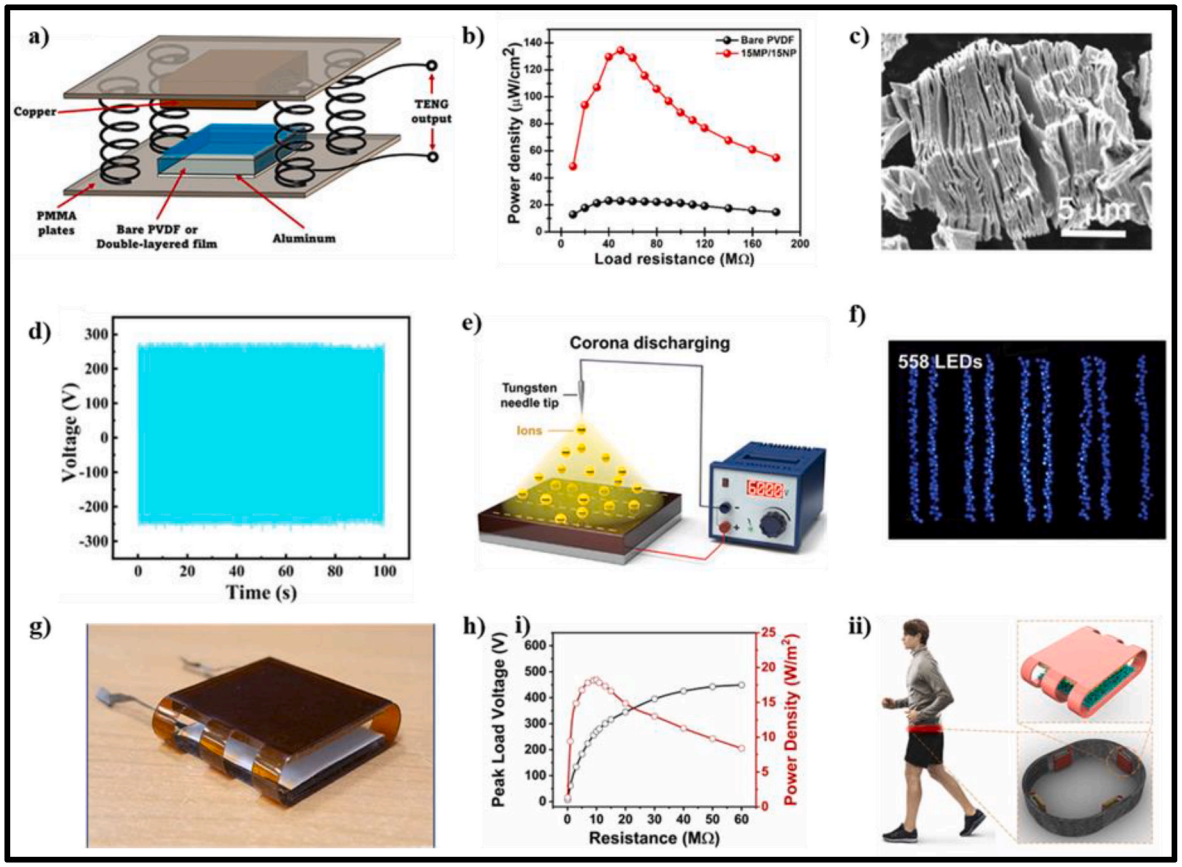

Fig. 7. a) TENG setup and different configurations of the electronegative layers. b) Output power density across external loads (Reprinted and adapted with permission from Ref. [142]. c) SEM image of multilayer MXene. d) Output voltage of the TENG sensor after 400 cycles at 4 Hz pulse. (Reprinted and adapted with permission from Ref. [144]), e) 3D schematic illustration of corona discharge treatment on SRP/MXene composite composites film f) Digital image demonstrating direct powering of 558 blue LEDs (3.3 V per unit) (Reprinted and adapted with permission from Ref. [145], g) optical image of fabricated VPCN-TENG device, h) (i) Peak load voltage and peak power density of the VPCN-TENG under various external loads (ii) Schematic of the proposed smart belt being worn by a volunteer. Real-time signal response of the VPCN-TENG sensor attached to the waist belt during (Reprinted and adapted with permission from Ref. [146]).

the triboelectric layer and electrode. The synergistic effect of these materials resulted in impressive output performance, with the device based on the CNT/MP11 hybrid film achieving a maximum voltage of 184.1 V and a current of 4.42 μA. The incorporation of Nb_2CT_x MXene in this hybrid structure contributed significantly to the TENG's high output, likely due to its excellent conductivity and unique surface properties. Additionally, the sensor demonstrated extremely sensitive, exhibiting a 20 ms response time, a 30 ms recovery time, and good stability across 400 cycles, as shown in Fig. 7(d) [144].

In another study, Cho and team used $Ti_3C_2T_x$ MXene to create a high-performance and sustainable TENG based on a SRP composite. They synthesized the MXene by etching aluminum layers from Ti_3AlC_2 powder using a LiF/HCl etchant, resulting in exfoliated single-layer MXene nanosheets stably dispersed in deionized water. The team then developed a novel approach to incorporate MXene into SRP by coating SRP powder with an aqueous MXene solution and hot-pressing the coated powder. This method created a uniform MXene segregated structure within the SRP matrix, maximizing the interfacial area between MXene and SRP while using minimal MXene content (below 1 wt%). They optimized the MXene content and film thickness to achieve outstanding TENG performance without electrical percolation. The resulting SRP/MXene composite-based TENG demonstrated significant improvements in output performance, requiring only 0.4 wt% of MXene to achieve the highest output. Compared to previous SRP-based TENGs (Table 4), this new composite showed 2.9 times higher peak voltage and 19.5 times higher peak current. After scaling up to a 4-inch wafer size and applying corona discharging, shown in Fig. 7(e), the TENG exhibited an 8.4 times improvement in peak power density, reaching 3.80 Wm^{-2}. The TENG turns on the 558 blue LEDs as shown in Fig. 7(f) [145]. Recently, Faruk and team prepared V_2CT_X by etching V_2AlC MAX phase with HCl and HF. The resulting V_2CT_X powder was then combined with PVDF-HFP to formulate a composite solution, which was electrospun to produce a V_2CT_X@PVDF-HFP composite nanofibrous (VPCN) mat. This mat served as a negative tribolayer in the TENG. The incorporation of V_2CT_X, with its abundant functional groups (-F, -O, and -OH), enhances the electronegativity of the composite. Additionally, the development of micro-capacitor networks within the polymer matrix resulted in a reduction of charge loss, thereby improving dielectric properties and enhancing electron-trapping capability. They developed the VPCN-TENG by pairing the VPCN mat with a PEO nanofibrous mat as the opposing triboelectric material, which is shown in Fig. 7(g). This configuration resulted in a remarkable power density of 18.2 W/m^2, surpassing a TENG utilizing pristine PVDF-HFP nanofibers by a factor of 3.5. VPCN-TENG's improved electrical output made it possible for it to efficiently transform biomechanical energy from a range of human movements into electrical power, which could run commercial devices like thermo-hygrometers and stopwatches. As a self-powered pressure sensor, the VPCN-TENG performed admirably, displaying an astounding sensitivity of 25.17 V/kPa in the 1–42 kPa range. The VPCN TENG acts as a motion sensor for tracking a variety of human activities by being incorporated in a belt, as shown in Fig. 7(h) [146].

Table 4
Performance metrics table of representative MXene-based TENGs.

Material System	Voltage	Current	Power Density	Ref.
MXene ($Ti_3C_2T_x$)/PVDF, with $NaNbO_3$/PDMS	150 V	4.3 μA	134 μW/cm^2	[142]
Nb_2CT_x MXene/CNT/PEDOT hybrid film	184.1 V	4.42 μA	420 μW	[144]
MXene/Sulfur-Rich Polymer (SRP) composite	2.9 × SRP baseline	19.5 × SRP baseline	3.8 W/m^2	[145]
V_2CT_x/PVDF-HFP nanofibrous composite	1180 V	120	18.2 W/m^2	[146]

5.1.4. Photocatalysis and electrocatalysis

Photocatalysis and electrocatalysis represent crucial methodologies for the conversion of solar and electrical energy into chemical fuels, with MXene-based materials assuming a progressively significant position in these fields [147,148]. In photocatalysis, MXene composites improve light absorption, facilitate charge separation, and offer numerous active sites, resulting in enhanced efficiencies for hydrogen evolution and CO_2 reduction [149]. The materials contribute to the minimization of electron-hole recombination and enhance the visible light response of semiconductor photocatalysts, facilitating a more efficient conversion of solar energy into chemical energy [150–153]. The advantages of electrocatalysis are enhanced by the exceptional electrical conductivity, adaptable structural characteristics, and plentiful active sites of MXenes. These features contribute to reduced overpotentials and improved selectivity in various reactions, including hydrogen evolution, oxygen evolution, and CO_2 reduction [148,154]. Electrocatalysts based on MXene frequently demonstrate improved stability and catalytic performance when they are doped or hybridized with metals or metal oxides, positioning them as promising options for sustainable energy applications [155]. Additionally, the tandem photoelectrocatalytic systems merge the benefits of photocatalysis and electrocatalysis using light absorption and electrochemical catalysis as a tandem system, producing a valuable chemical fuel, such as ethanol, methanol or even CO which can be used in steel production manufacturing, that could potentially replace fossil fuels [156–161], as seen in Fig. 8.

This innovative system has no CO_2 concentration limits due to solubility and diffusion across the double layer, and competing water chemisorption is much reduced [163] (see Fig. 9). These systems employ MXene-based materials to enhance charge carrier separation and transport, consequently enhancing the efficiency and selectivity of CO_2 reduction and water splitting reactions. The combined effects in MXene-containing photoelectrodes promote swift electron transfer and efficient use of photogenerated carriers, leading to increased product yields and enhanced stability during operational conditions [162]. However, catalytic photocorrosion and compatibility affect tandem photoelectrocatalysis efficiency, stability, and selectivity, as seen in Fig. 6. Contact with the catalyst could change the reaction pathway, which could change the selectivity of the product and the effectiveness of the photoelectrocatalytic CO_2 reduction. Addressing these issues is necessary to create highly stable, efficient, and selective photoelectrocatalytic CO_2 reduction systems. For example, in some research studies, methanol content increased significantly compared to previous tests, indicating improved reaction conditions [164–167]. Ethanol production explains this improvement in photoelectrochemical systems [168]. These systems have more methanol and less ethanol, at least six times higher than other systems, such as photocatalysis and electrocatalysis [169]. Recent advances encompass the creation of heterojunctions and composite structures that enhance light harvesting and catalytic interfaces, advancing the performance of photoelectrocatalytic devices toward practical solar fuel production [170]. Despite these advances, challenges such as material stability suppression of electron-hole recombination, and large-scale fabrication persist, guiding continuous research in this dynamic field.

5.2. MXene-based materials for energy storage

MXenes, a family of 2D transition metal carbides and nitrides, have emerged as highly promising materials for ES devices due to their unique structural and electrochemical properties. As illustrated in Fig. 6, MXenes are synthesized by selectively etching the 'A' layer from MAX phases, followed by delamination into few-layered nanosheets [171,172]. These nanosheets can be formulated into stable inks, enabling advanced printing techniques such as IJP, screen, gravure, DIW, and 3D printing to fabricate customized electrode patterns on flexible substrates [173–175]. This printing capability not only allows for precise control of material deposition over flexible or rigid substrates but also supports

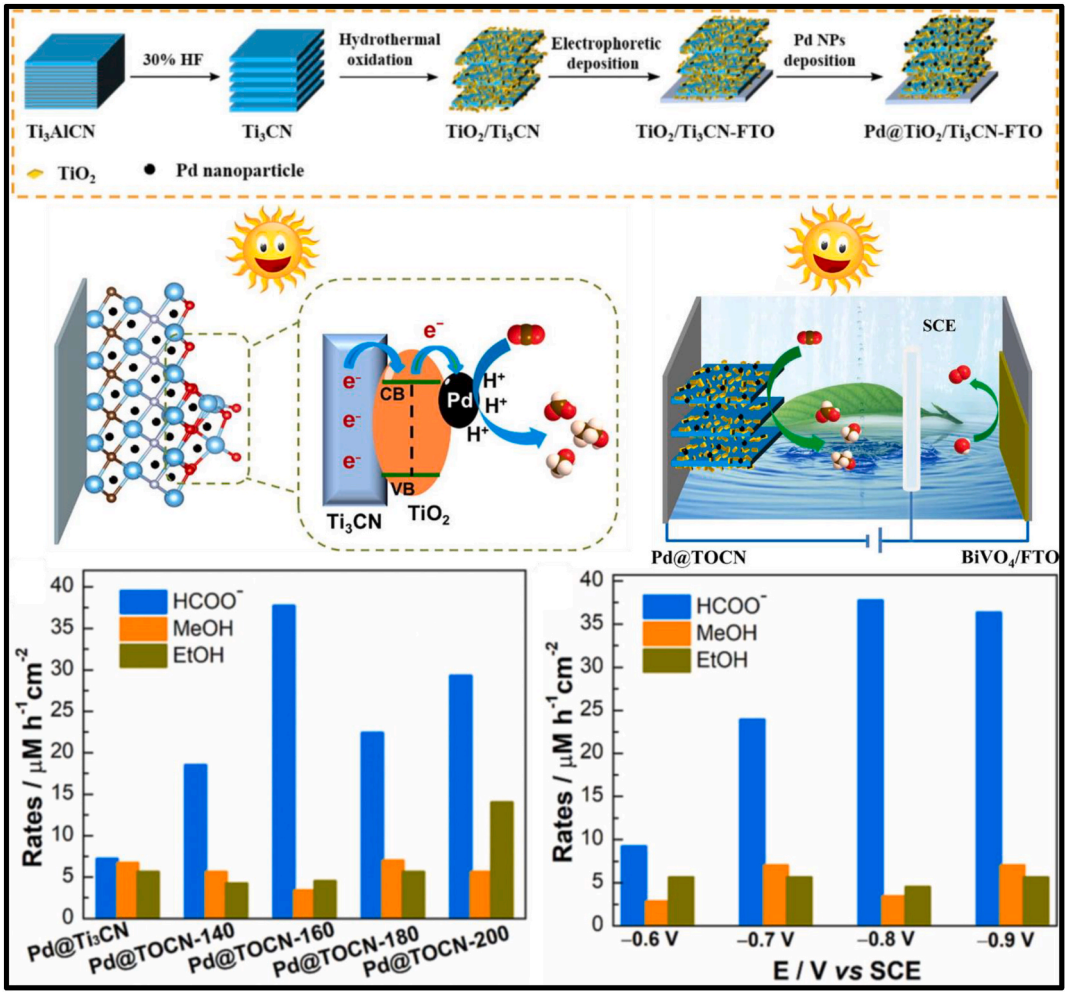

Fig. 8. CO_2 photoelectrocatalytic performance over Pd@TiO_2/Ti_3CN MXene composites. Reprinted and adapted with permission from [162].

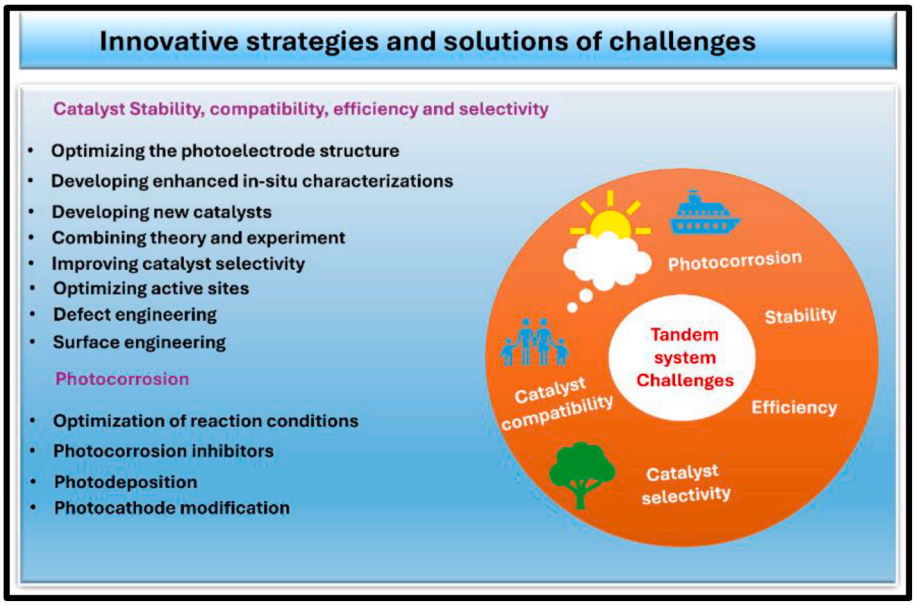

Fig. 9. A schematic diagram illustrates the evaluation parameters for issues related to photoelectrocatalytic CO_2 reduction, along with associated innovative strategies and solutions.

scalable and cost-effective production of ES devices [176,177]. The high electrical conductivity, tunable surface chemistry, and mechanical flexibility of MXenes make them ideal candidates for SCs and batteries, where they can enhance charge transport, storage capacity, and cycling stability. Overall, MXene-based printable electronics offers a transformative platform for the development of next-generation, lightweight, and flexible ES systems.

The formulation of MXene inks for printed supercapacitors has to precisely meet the requirements of each printing technique, as these parameters directly influence device performance and scalability. For example, IJP, operating at a speed of approximately 1 m/min, requires low-viscosity MXene inks (1–20 cP) and small particle sizes, typically below 200 nm depending on the cartridge nozzle size, with surface tension values between 25 and 40 mN/m to ensure smooth jetting and prevent nozzle clogging. This method produces films with thicknesses ranging from 0.5 to 5 μm and achieves high resolution (10–50 μm). Furthermore, substrates such as PET and polyimide are commonly treated with plasma or UV-ozone to enhance wettability, and post-printing steps involve drying or annealing at temperatures between 80 and 200 °C [178–181].

Spray printing such as the aerosol jet printer operates at high speed of~20 m/min and also utilizes low-viscosity inks (1–10 cP). It is capable of producing films with thicknesses from 5 to 100 μm and moderate resolution (50–200 μm). The technique is well-suited for rapid, large-area deposition, but requires careful control of ink fluidity and colloidal stability to avoid nozzle clogging and aggregation. Spray-printed MXene supercapacitors have demonstrated high areal and volumetric capacitance, with recent studies reporting in literature [182,183]. However, challenges such as nanosheet restacking and drying dynamics have to be managed to maintain film uniformity and optimal device performance [184–186].

Screen printing operates with significantly higher viscosities, ranging from 100 to 107 mPa s, and accommodates larger MXene particle sizes up to 10 μm. This technique produces relatively thick films, typically between 10 and 100 μm, with good resolution in the range of 30–100 μm. However, screen printing faces limitations due to low solid loading in the inks, high additives content and the tendency of MXene nanosheets to restack, which can negatively impact the areal capacitance of the resulting supercapacitor electrodes. To address adhesion and film quality, standard protocols include substrate pretreatments and post-printing drying or annealing at temperatures between 100 and 300 °C [186].

For 3D printing, the requirements are even more demanding, with MXene inks needing to be highly viscous and exhibit shear-thinning behavior, with viscosities typically between 106 and 108 mPa s. These inks are often formulated with additives such as cellulose nanofibers or carbon nanotubes, which help prevent nanosheet restacking and improve printability. The 3D printing process can produce films thicker than 50 μm, with resolutions ranging from 10 to 100 μm. To enhance adhesion, substrates may be heated or functionalized, and post-processing steps such as drying, sintering, or curing are commonly employed to ensure structural integrity and optimal electrochemical performance [187].

R2R gravure printing, which is well suited for large-area device fabrication, requires MXene inks with moderate viscosity (50–500 mPa s), excellent colloidal stability, and particle sizes below 500 nm to ensure uniform transfer from the engraved cylinder to the substrate. Achieving good pattern fidelity (10–50 μm) and film thickness (10–100 μm) depends on matching the surface energy of the ink and substrate, while post-printing drying is typically performed at 80–150 °C [177].

The choice of solvent, such as aqueous and organic solvents, and the use of additives such as binders, surfactants, and rheology modifiers are carefully optimized to balance printability, film formation, and device performance, while minimizing MXene oxidation and restacking. Notably, recent advances have demonstrated the feasibility of additive-free MXene inks, which can further simplify processing and enhance electrochemical performance by avoiding unwanted side reactions or impurities [183].

5.2.1. MXene-based supercapacitors

MXenes, particularly $Ti_3C_2T_x$, have developed as promising candidates for printed SCs, owing to their exceptional electrochemical properties. These include superior conductivity, a large surface area, and rapid ion diffusion rates, making them ideal for advanced ES applications [188]. The 2D layered architecture of MXenes, combined with their surface functional groups such as OH–, F–, and O–, enhances redox activity and enables high energy density, which are critical properties for ES [189]. This structural and chemical interaction improves charge transfer kinetics and ion accessibility, positioning MXenes like $Ti_3C_2T_x$ as the first candidate in the next generation of printed ES systems [190]. Due to these exceptional properties, the MXene ink was used to print SCs using different printing techniques, such as screen, 3D, IJP, and DIW [143,191–193]. This is why formulating MXene-based inks with good rheological properties for printing and high electrochemical performance is a massive step forward in the research of MXene-based printed SCs [191,194,195]. Therefore, to formulate an ink of MXene, different surfactants or polymers can be used to adjust the rheological properties [194,195].

The assembly of 2D materials, specifically MXene, into functional 3D aerogels through the application of 3D printing technologies is attracting high attention. Tetik et al. [196] attributed this interest to the straightforward fabrication process, the ability to customize geometry and physical properties, resulting enhancement in electrochemical performance. In their investigation, the researchers employed a hybrid approach combining unidirectional freeze casting with inkjet-based 3D printing to construct porous aerogels at the macroscopic scale. These aerogels were characterized by precisely oriented $Ti_3C_2T_x$ MXene sheets aligned vertically, enabling meticulous control of the internal microstructure and orientation. The resulting aerogels exhibited improved electromechanical characteristics, demonstrated by their resilience in recovering their original form after compression of nearly 50 %. Notably, the electrical conductivity of the printed MXene structures remained stable even under repeated compressive stress. Furthermore, by inkjet-printed MXene sheets aligned horizontally as a current collector, the electrochemical performance was significantly enhanced, attributed mainly to increased porosity and optimized ion transport.

μSCs extensively utilize MXenes due to their superior conductivity and hydrophilic properties for flexible wearable electronics. However, MXene-based μSCs usually have low capacitance and poor rate performance due to limited porosity and ion diffusion pathways. Therefore, Wang et al. investigated the preparation of MXene inks with large interlayer spacing between the layers, which speeds up the ion diffusion of lithium ions between the layers [197]. Lithium-ion-introduced MXene inks were utilized via screen printing for scalable fabrication of μSCs. By incorporating a concentrated aqueous electrolyte (21 M LiTFSI) and employing an optimized electrode structure, the device achieved a wide effective voltage range. It exhibited an outstanding areal capacitance of 252 mF cm^{-2} with an enhanced capacitance retention of 80 %. Additionally, the fabricated μSC demonstrated impressive cycling durability, retaining approximately 98.4 % of its original capacitance even after 10,000 charge-discharge cycles. The device also displayed significant mechanical flexibility, highlighting its strong potential for use in wearable smart electronic applications.

With the fast development of wearable, flexible, and implantable microelectronics, there is an increasing demand for compact and *integrated* ES devices possessing robust mechanical properties, capable of working under high voltage conditions, and easily adaptable for integration into IoT systems. Zheng et al. proposed a systematic approach for developing KIμSCs by employing MXene-derived KTO nanorods as the anode, while a porous AG as the cathode, specifically aimed at powering a highly sensitive pressure sensor [198]. The sophisticated nanostructure of KTO nanorods enabled substantial potassium-ion storage

capacity (145 mAh g^{-1}). Notably, the fabricated KIμSCs exhibited an extended working voltage window of 3.8 V, outperforming previous μSC designs. Furthermore, KIμSCs reached an impressive volumetric energy density of 34.1 mWh cm^{-3}, along with excellent rate capability and substantial capacitance retention. These superior performance results from the dominant capacitive storage mechanism and minimal structural changes during the reversible intercalation/deintercalation of potassium ions within KTO, as well as from the efficient adsorption/desorption processes of LiTFSI anions on the AG cathode. When integrated with a wireless pressure sensor on a flexible substrate, a KIμSC effectively monitors body movement.

To enhance μSC performance, improving the 3D printing capability of MXene inks and addressing the nanosheet restacking issue are crucial. In response, Zhou et al. formulated a composite ink incorporating MXene [191], MWCNTs, and CNFs [199]. They subsequently fabricated precise, customizable, freestanding electrodes using a controlled DIW method. Integrating conductive MWCNTs and hydrophilic CNFs significantly improved the ink's rheological characteristics, resulting in a more cohesive internal structure and expanded interlayer spacing within the MXene nanosheets. Consequently, the 3D-printed flexible electrodes exhibited stable electrical conductivity, increased accessible surface area, enhanced wettability, and superior electrochemical performance. Furthermore, the authors prepared a CNF/PAM hydrogel electrolyte via *in situ* radical polymerization. Using this electrolyte in combination with two 3D-printed IDE, they developed a flexible IDE μSC exhibiting notable energy density (21.7 μWh cm^{-2}) and power density (0.3 mW cm^{-2}).

The rapid progress of wearable electronics demands higher-performing power systems with features such as flexibility, easy attachment and detachment, reliable output, and prolonged lifespan. Given the limited capacity of typical ES devices, integrating energy harvesting with storage becomes an effective solution for improved performance. Zhou et al. developed a flexible, wearable, and wireless energy supply system combining a PUAHs and MSSSs into a comfortable wristband suitable for continuous usage [200]. The MSSS component comprises a finger-shaped carbon cloth framework coated with $Ti_3C_2T_x$ nanosheets as electrode material and a PVA/H_3PO_4 gel electrolyte, achieving remarkable energy density (58.74 Wh kg^{-1}) and exceptional cycle stability, maintaining 99.37 % of its capacity after 10,000 cycles. The wireless charging module consists of a two-dimensional, stretchable piezoelectric array, utilizing high-efficiency 1–3 composite elements and serpentine-shaped electrodes, which facilitate wireless energy transmission via ultrasonic waves. This module attains a maximum power density of 1.56 W cm^{-2} and an output voltage of 20.75 V. With a compact thickness of merely 2 mm, the integrated PUAH-MSSS system delivers superior energy harvesting and storage capabilities, excellent mechanical flexibility, and consistent cyclic performance.

The DIW of functional inks is increasingly critical for numerous fields, including EES, healthcare, and smart electronics. However, existing printable ink formulations still have limitations, often relying on surfactants, additives, or higher ink concentrations, complicating production and negatively affecting print quality. Zhang et al. developed two distinct types of 2D $Ti_3C_2T_x$ MXene inks, one aqueous for extrusion printing and one organic for inkjet printing [191]. Remarkably, these formulations avoided additives and binary solvent mixtures altogether. They demonstrated printing high-resolution structures composed solely of MXene, including μSCs, conductive pathways, and ohmic resistors, on untreated plastic and paper substrates. These MXene-based printed structures exhibited superior uniformity and resolution. Furthermore, μSCs fabricated entirely from printed MXene inks displayed volumetric capacitance and energy densities significantly exceeding those achieved with conventional extrusion- and inkjet-printed active materials. Their DIW approach emphasizes the viability of additive-free MXene inks for scalable and efficient fabrication of components suited to advanced printable electronics applications (see Fig. 10).

Sun et al. explored the feasibility of inkjet printing to fabricate intricate three-dimensional structures, specifically developing a novel porous network composed of N-MXene and $NiCo_2S_4$ for high-performance hybrid μSCs, as illustrated in Fig. 11 [201]. Utilizing XPS, they identified a unique bridging interaction between nickel and oxygen atoms. DFT calculations revealed that oxygen atoms in N-MXene effectively attract electrons from nickel atoms within $NiCo_2S_4$, leading to electron redistribution throughout the composite structure. This electron redistribution enhances the overall structural stability of the 3D N-MXene/$NiCo_2S_4$ composite. Remarkably, the developed μSCs retained approximately 99.1 % of their initial capacitance after 25,000 charge-discharge cycles, benefiting from the continuous exposure of active sites in the porous architecture. The μSCs also demonstrated an extensive potential window, high volumetric capacitance, and an impressive energy density of 1.6 V, 342.4 mWh cm^{-3}, and 983.9 F cm^{-3}, respectively, surpassing previously reported performances. Additionally, this research proposed an innovative method using high-precision inkjet printing to precisely control the morphology and internal microstructure of electrodes, thereby significantly enhancing the electrochemical properties of μSCs.

μSCs have gained attention for their outstanding power density and prolonged operational lifespan, making them suitable as integrated ES units in electronic devices. Dey et al. developed an IDE interdigitated μSC design fabricated on transparent and flexible substrates by employing a precisely patterned mask combined with screen-printing technology [202]. They utilized two distinct electrode materials: $Ti_3C_2T_x$ MXene and nickel selenide (NiSe). The layered structure of MXene facilitated rapid ion diffusion within the IDE arrangement, whereas NiSe nanoparticles contributed enhanced surface area and increased active sites. The resulting asymmetric NiSe/MXene μSC (NiSe/MXene A-μSC) operated within an aqueous electrolyte over a voltage range of 0–1.8 V, maintaining 72 % capacitance retention after 1000 charge-discharge cycles. It exhibited a notable volumetric energy density of 117.6 mWh cm^{-3} and a power density of 1285.7 mW cm^{-3}. Moreover, the μSCs demonstrated robust mechanical flexibility under bending conditions. This work highlights the potential of integrating planar $Ti_3C_2T_x$ MXene and NiSe electrodes in aqueous-based asymmetric μSCs, using MXene as the negative electrode and NiSe as the positive electrode, to enhance both energy density and voltage window, fulfilling essential criteria for powering advanced electronic systems.

Despite substantial advancements in using inkjet printing to create scalable and customizable power sources, developing environmentally sustainable aqueous inks remains challenging. Ma et al. addressed this by introducing an aqueous MXene/PEDOT:PSS (MP) hybrid ink with tunable viscosity, enabling direct fabrication of high-performance MP-based-μSCs [203]. These printed devices demonstrated exceptional electrochemical properties, ease of integration, and significant adaptability, making them highly promising for industrial-scale applications in self-powered integrated electronics. Specifically, the MP-μSCs achieved a volumetric capacitance of 754 F cm^{-3} and delivered an energy density of 9.4 mWh cm^{-3}. Such notable performance arises from integrating the highly conductive PH1000 polymer into MXene, effectively preventing the restacking of MXene nanosheets and enhancing rapid electron and ion mobility within the electrode structure. By arranging 60 MP-μSC cells in series, they successfully increased the overall working voltage to 36 V, attaining a notable areal voltage of 5.4 V cm^{-2}. Additionally, the integrated system incorporated a printed temperature sensor and flexible solar cells, demonstrating a notable 2 % response sensitivity and superior mechanical flexibility. The developed MXene-based inks thus provide extensive potential for miniaturizing and fabricating novel, flexible microsystems that seamlessly combine harvesting, energy storage, and utilization in printed electronic devices.

3D printing has emerged as an attractive manufacturing technique for producing supercapacitor electrodes, enabling precise and customizable fabrication of complex electrode designs, which significantly enhances device performance. However, limitations in the conductivity and electrochemical performance of electrodes created through 3D

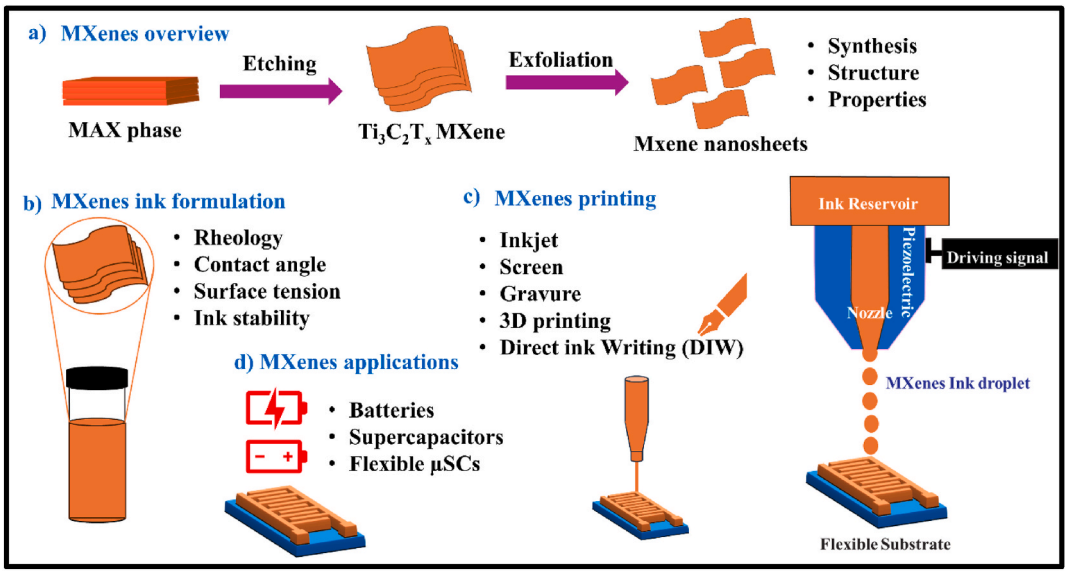

Fig. 10. The schematic illustration provides a comprehensive overview of the MXene-based printable electronics process, highlighting each stage from material preparation to final application.

printing persist due to the lack of suitably conductive materials. To overcome this limitation, Mappoli et al. enhanced the electrical properties of 3D-PnC activated electrodes by depositing $Ti_3C_2T_x$ MXene onto their surfaces [204]. Subsequently, they developed a solid-state asymmetric supercapacitor employing the 3D-PnC/$Ti_3C_2T_x$ composite as the negative electrode and 3D-PnC@PANI as the positive electrode. This configuration notably enhanced the overall operating voltage range, areal capacitance, and energy density of the resulting asymmetric supercapacitor device.

Sarfraz et al. conducted a theoretical investigation into the structural and electronic characteristics of homo-bilayer and hetero-trilayer systems. The study covered C_Q, density of states and surface charge, average C_Q, work function, charge redistribution (both integrated and isosurface), and bader charge analysis [205]. The negative binding energies confirm that all the proposed configurations are energetically stable. Notably, introducing a 3d transition metal at the interface substantially enhances both C_Q and total stored charge (Q), with hetero-trilayers showing superior performance compared to homo-bilayers. In aqueous environments, most bi- and tri-layer systems exhibit asymmetric charge behaviour, except for M/V/M, M/Cu/M, and M/Fe/M trilayers. Among these, M/Zn/M demonstrates the highest cathodic charge capacity (906.75 μC cm^{-2}), while M/Fe/M stands out as the best-performing anode (925 μC cm^{-2}). For ionic and organic systems, all bilayers display asymmetric behavior except for M/V/M. Here, M/Mn/M achieves the highest anode charge (1538.5 μC cm^{-2}), and M/Fe/M again ranks as the most efficient cathode (1416.4 μC cm^{-2}). Interestingly, the electrode role of certain hetero-trilayers shifts with voltage conditions. M/Fe/M and M/Cu/M transition from symmetrical supercapacitor electrodes to cathodic materials in asymmetrical configurations, whereas M/Ti/M switches from cathode to anode functionality. Overall, M/Fe/M, M/Mn/M, and M/Zn/M hetero-trilayers exhibit notably high CQ, surface charge accumulation, and electrochemical energy and power densities, indicating strong potential for advanced energy storage applications. The integration of supercapacitors into self-powered sensors and biosensors offers a promising solution to the economic, miniaturization, biocompatibility, and disposal challenges associated with batteries, while showcasing recent advances, fabrication techniques, diverse energy harvesting approaches, and future prospects for improved biomedical and analytical applications [53,206].

5.2.2. *MXene-based batteries*

In the area of printed batteries, MXene-based materials, especially $Ti_3C_2T_x$, have received considerable attention due to their exceptional electrical conductivity, mechanical flexibility, and versatile surface chemistry. Two-dimensional MXenes are particularly suitable for ES applications, including LIBs, as they can efficiently serve as both electrodes and current collectors [207]. Techniques such as inkjet and 3D printing leverage MXene's high conductivity and rapid ionic transport to fabricate flexible and lightweight battery components. The use of MXene in printed batteries provides significant benefits, such as an extensive surface area and excellent ion intercalation capabilities, which enhance ES capacity and enable faster charging. For example, inkjet-printed $Ti_3C_2T_x$ MXene current collectors combined with LTO and LFP electrodes have demonstrated superior mechanical flexibility, retaining stable electrochemical performance even under bending conditions, making them highly suitable for wearable electronics and flexible device applications [208,209].

Ramachandran et al. [49] examine the role of MOF/MXene hybrid materials in enhancing ZAB performance, detailing ZAB architecture, ORR and OER mechanisms, synthesis strategies, and design considerations for optimizing catalytic activity, stability, and gas diffusion, while addressing kinetic challenges and electrolyte effects on energy efficiency, power density, and cycling durability. It concludes with forward-looking strategies to overcome current limitations—such as reaction kinetics and material robustness—highlighting the transformative potential of MOF/MXene hybrids to drive the commercial adoption of high-performance, sustainable ZABs.

Vanadium-based materials are considered promising electrode candidates for ES systems due to their low cost, abundant availability, and diverse chemical and structural characteristics. Among them, vanadium compounds with layered architecture have attracted significant attention for exhibiting efficient multielectron redox activity. In a study by Myint et al., a VM incorporating TiO_2@Ti_3C_2 MXene was synthesized through the *in situ* thermal decomposition of a $VO_2(OH)/Ti_3C_2$ mixture, as illustrated in Fig. 12 [210]. Structural analysis confirmed the formation of orthorhombic V_2O_5 nanostructures along with nanocrystalline TiO_2 supported on Ti_3C_2 layers. The optimized composite containing 5 % MXene (VM5) achieved a specific capacity of 460 mAh g^{-1} at 0.1 A g^{-1} and 290 mAh g^{-1} at 1 A g^{-1}, maintaining an average coulombic efficiency of 98.5 %. The integration of Ti_3C_2 was found to reduce charge transfer resistance, improving the electrochemical kinetics. VM5

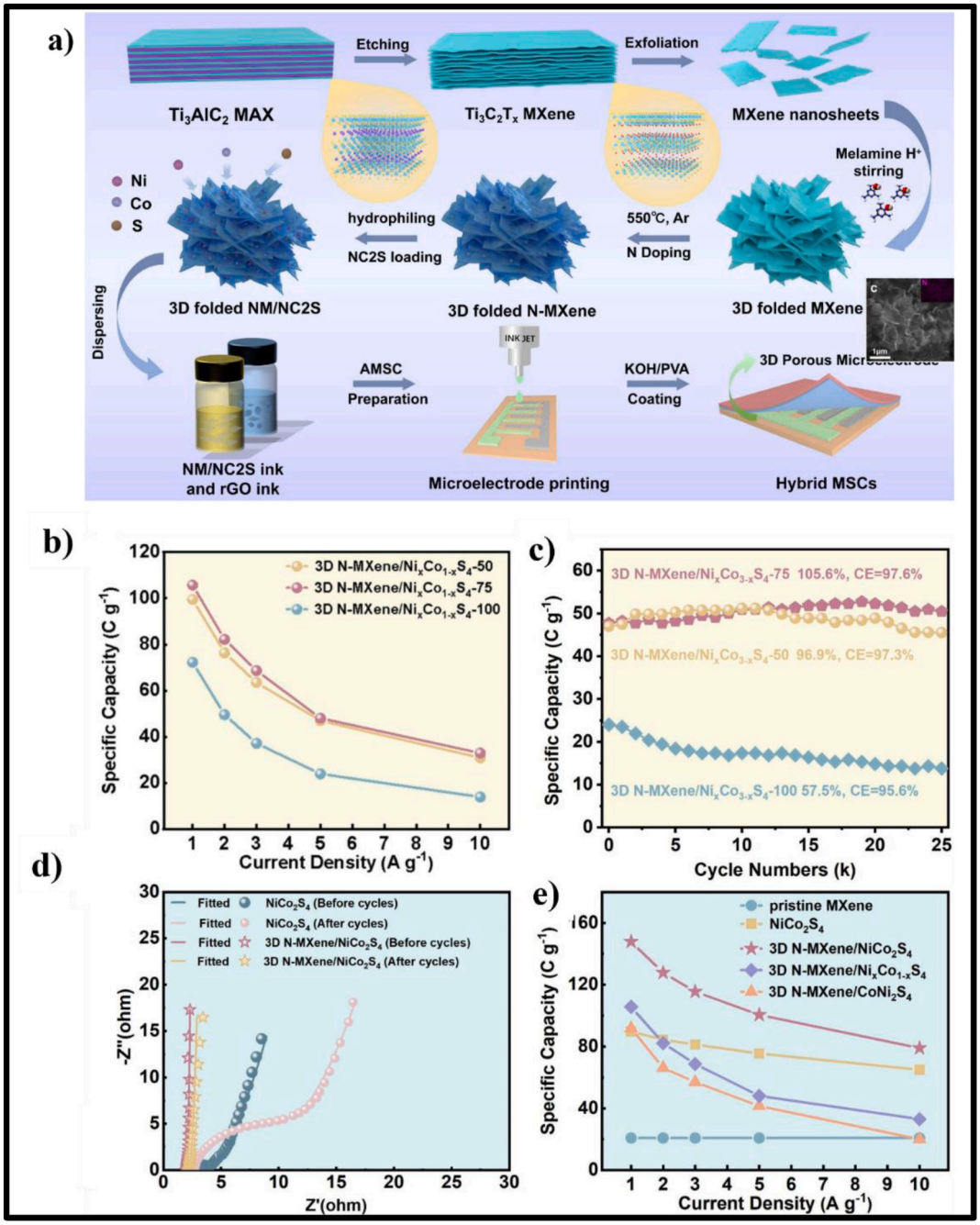

Fig. 11. a) Schematic illustration of the fabrication of the 3D pleated N-MXene/$NiCo_2S_4$ for inkjet printing and the assembly process of HμSCs; b) Specific capacity of 3D N-MXene/$Ni_xCo_{3-x}S_4$-50/75/100 electrodes at different current densities. c) The capacity retention rate of 3D N-MXene/$Ni_xCo_{3-x}S_4$-50/75/100 electrodes. d) EIS spectra of $NiCo_2S_4$ and 3D N-MXene/$NiCo_2S_4$ electrodes. e) The Specific capacity of pristine MXene, $NiCo_2S_4$, 3D N-MXene/$Ni_xCo_{3-x}S_4$, 3D N-MXene/$NiCo_2S_4$, and 3D N-MXene/$CoNi_2S_4$. Reprinted and adapted with permission from Ref. [201]).

also demonstrated decent cycling performance, with 62 % capacity retention over 500 cycles at 1 A g^{-1}, corresponding to a per-cycle capacity fade of 0.22 %. Charge storage behavior analyzed using Dunn's method revealed that 72 % of the capacity originates from surface-controlled capacitive processes, while 28 % arises from diffusion-driven intercalation at a scan rate of 0.4 mV/s, underscoring the material's potential as a high-performance pseudocapacitive electrode for lithium-ion batteries.

ES plays a crucial role in powering electronic devices, and inkjet printing has emerged as a promising technique for battery fabrication. This method leverages the benefits of thin-film technologies, such as lightweight construction, mechanical flexibility, and ease of integration into various systems. As the IoT sector continues to grow rapidly, there is increasing interest in developing smart, seamlessly integrated electronic components. A key challenge in producing fully inkjet-printed batteries lies in the fabrication of CCs, which are responsible for providing mechanical support to the electrodes while ensuring efficient electrical connectivity to the external circuit. To address this issue, Viviani et al. introduced a straightforward ink formulation based on $Ti_3C_2T_x$ MXene—an electrically conductive and hydrophilic material, suitable for printing current collectors [193]. Their study included an evaluation of substrate compatibility and device configuration requirements. The resulting battery was entirely printed and demonstrated excellent flexibility, maintaining its performance even under mechanical

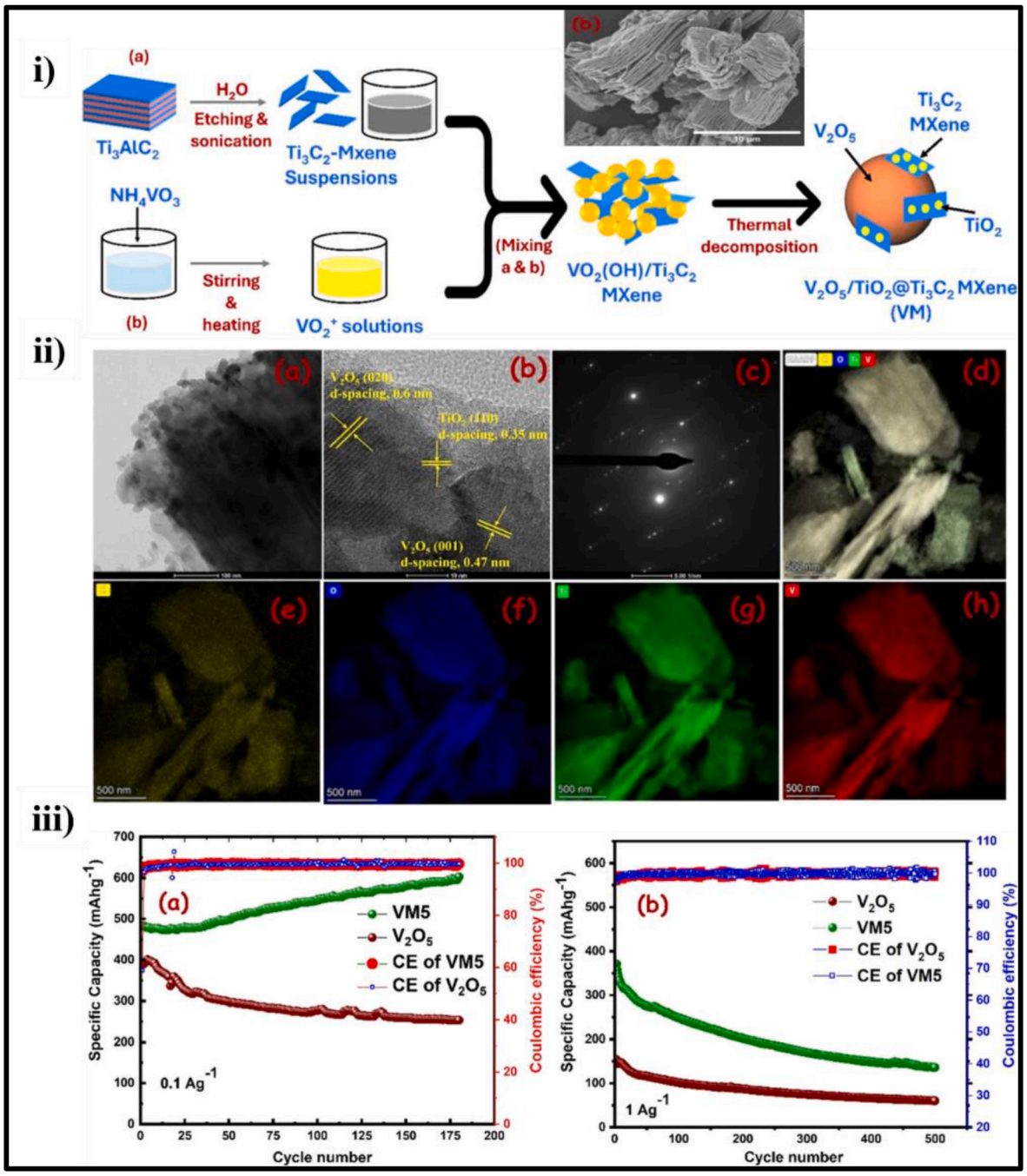

Fig. 12. i) Schematic Representation of the Fabrication of the VM Composite Electrode via In Situ Thermal Decomposition of the $VO_2(OH)/Ti_3C_2$ Mixture: (a) Preparation of Ti_3C_2-MXene Suspensions and (b) Preparation of VO_2^+ Solutions; ii) (a) TEM, (b) HR-TEM, (c) ED, and (d) HAADS-STEM images of VM5. (e–h) EDS elemental mapping; and iii) Cyclic performance of V_2O_5 and VM5 (a) at 0.1 Ag–1 and (b) at 1 Ag–1 (Reprinted and adapted with permission from Ref. [210]).

deformation. The results highlight the potential of $Ti_3C_2T_x$ MXene as a candidate for flexible printed CCs. However, for real-world applications, further improvement in the electrochemical properties, particularly the areal capacity, is still necessary.

Zn metal anodes have garnered considerable attention for use in AZIBs due to their high theoretical capacity, low redox potential, and affordability. Despite these advantages, issues such as uncontrollable dendrite formation and parasitic side reactions hinder their reversibility and lead to rapid battery degradation. To address these challenges, Zhu et al. developed a protective layer composed of PVDF and MXene nanosheets using a 3D printing approach [211]. This technique promoted the transformation of PVDF from the non-polar α-phase to the electroactive β-phase, thereby enhancing its ferroelectric characteristics. The presence of MXene facilitated this phase transition and contributed to a more homogeneous distribution of Zn^{2+} ions, promoting uniform zinc deposition. Anodes equipped with the PVDF-MXene-Zn exhibited highly stable zinc plating and stripping behavior, maintaining low voltage hysteresis at 1.0 mA cm^{-2} with a capacity of 1.0 mAh cm^{-2} over 4200 h. These anodes also demonstrated strong rate capability up to 10 mA cm^{-2}. Furthermore, pairing MnO_2 and activated carbon with these modified anodes led to the fabrication of Zn-MnO_2 batteries and zinc-ion capacitors with significantly improved cycling performance. The study presents an innovative approach to enhance the stability and practicality of ZIBs through the effective protection of the zinc anode.

Zn-P anodes offer notable advantages over traditional zinc foil anodes, particularly in terms of adaptability and ease of processing. However, their inherently rough and high-surface-area structure tends to promote uncontrolled dendritic growth and undesirable side reactions. To overcome these challenges, Lu et al. employed a microfluidic-assisted 3D printing method to construct a corrosion-resistant Zn-P-based anode, incorporating a functional layer composed of an MXene/Cu-THBQ heterostructure [212]. This protective layer exhibits excellent corrosion resistance and strong Zn^{2+} adsorption capabilities, which collectively help regulate zinc ion transport and suppress the HER during repeated plating/stripping cycles. As a result, the symmetric cell utilizing this engineered Zn-P/MXene/Cu-THBQ anode demonstrated outstanding cycling stability, maintaining performance for 1800 h at a current density of 2 mA cm^{-2} and a capacity of 1 mAh cm^{-2}. Additionally, a full zinc-organic battery incorporating an organic cathode based on 4-hydroxy-2,2,6,6-tetramethylpiperidine-1-oxyl tethered to graphene exhibited high reversible capacity and excellent cycle life, further supporting the practical viability of the proposed anode design. Table 5 provided an overview of MXene-based devices, summarizing key performance metrics, including power density, capacitance, and energy density; across different material systems and device configurations, with particular emphasis on the performance enhancements achieved through MXene incorporation.

6. Conclusion and future perspectives

In summary, research on MAX phases and MXenes has rapidly advanced since their initial exploration in 2011. Among the MXene family, $Ti_3C_2T_x$ has emerged as a prominent material in the energy harvesting field. As discussed in this paper, various preparation techniques, including HF and non-HF methods, have been adopted for the synthesis of MXenes and their composites. Benefiting from their large surface area, inherent hydrophilic properties, abundant surface termination groups, and excellent metallic conductivity, MXene-based composites have been extensively studied for energy harvesting and storage applications, such as batteries, supercapacitors, TENGs, and solar cells. However, the comparison between the extensive studies of MXenes and other 2D materials remains in its preliminary stages, and several urgent issues must be addressed before MXenes can be scaled up for commercial applications (Fig. 13).

First, most methods for preparing MXenes involve complex steps, which are time-consuming, toxic, and limited by the challenges of bottom-up techniques. There is a pressing need for cost-effective, environmentally friendly, and efficient methods for large-scale production.

Second, uniform surface termination functional groups have yet to be consistently prepared, which affects the efficiency and electronic properties of MXenes in energy storage applications. Therefore, it is necessary to develop and design effective strategies to optimize and accurately control the functional groups of MXenes, with an emphasis on qualitatively and quantitatively understanding the T_x groups. Furthermore, experimental work and machine learning techniques should be combined to gain a deeper understanding of the fundamentals of MXene surface functionalization.

Third, energy harvesting applications typically use accordion-like and few-layered structures, which often aggregate and agglomerate during the storage process. To address this issue, further investigation of quantum dots and 3D architecture is needed.

Finally, MXenes are well known to be easily oxidized in air and humid environments due to their metallic conductivity and the tendency of Ti atoms to lose electrons in the presence of oxygen, which negatively affects electron transport and charge carrier separation. To address this challenge, novel strategies, such as coating with carbon materials, semiconductors, or polymers, have been explored to enhance the stability of MXenes. If these bottlenecks can be resolved, the potential of

Table 5
Overview of MXene-based devices, summarizing key performance metrics.

Device Materials (Application)	Technique	Ink solvent	Viscosity	Electrolyte	Cell Type/ (PW*)	Capacitance	Energy/Power density	Capacitance retention% (Cycle)	Ref.
$Ti_3C_2T_x$ MXene	AJP	DI water	~4 cP	PVA/H_2SO_4	(IDE) (1.6 V)	122 mF cm^{-2}	–	86.22 % (10,000)	[183]
MXene/ Conductive Cellulose	3D printing	DI water	5 Pa s	LiCl/SiO_2 gel electrolyte	(IDE) (1.6 V)	3.12 F cm^{-2}	1.25 mWh cm^{-2}	95 % (10,000)	[213]
MXene/CNT composite	3D printing	DI water	10291.1 Pa s	PVA/H_2SO_4	(IDE) (0.8 V)	1249.3 mF cm^{-2}	111 μWh cm^{-2}/ 0.4 mW cm^{-2}	82 % (5000) at 10 mA cm^{-2}	[214]
VCG//ACG/ CG/MXene ASC devices	3D printing	DI water	0.5 pa.s at 100 S^{-1}	PVA/KOH	(IDE) (0.8 V)	205.57 mF cm^{-2}	60.03 μWh cm^{-2}/0.174 W cm^{-2}	70 % (200) at 3.6 mA cm^{-2}	[215]
V_2CT_x	inkjet printing	DI water/ anhydrous ethanol	7.8 mPa s	PVA/H_2SO_4	(0.4 V)	23.4 μF cm^{-2} at 5 mV s^{-1}	–	83 % (7000)	[216]
titanium carbide ($Ti_3C_2T_x$)/Ag NWs	DIW	(PEDOT:PSS)/ EG/DI water	–	H_3PO_4/PVA	(IDE) (1 V)	8.34 mF cm^{-2}	1.5 μW h cm^{-2}/0.6 mW cm^{-2}	88 % (10000)	[217]
CoNi-PBA/ MXene	Screen printing	7 wt% ethyl cellulose solution in n-propanol	0.9 Pa s at 1000 S^{-1}	Acrylamide, ammonium persulfate, N, N methylenebisacrylamide, and NaCl/DI water	(1.6 V)	245.36 mF cm^{-2}	0.087 mWh cm^{-2}/16.00 mW cm^{-2}	77.52 % (16000)	[218]
MXene	Screen printing	DI water	–	H_2SO_4/PVA gel	(IDE) (0.6 V)	4979.2 mF cm^{-2}	62.2 μWh cm^{-2}/0.19 mW cm^{-2}	80.53 % (3500)	[219]
NiSe/MXene A-MSC	Screen printing	ethyl cellulose/ terpineol solvent	1200 Pa s at 1000 S^{-1}	CMC-NaOH gel electrolyte	(IDE) (1.8 V)	65.4 mA h cm^{-3} (91.6 μA h cm^{-2}) at 0.4 mA	117.6 mW h cm^{-3}/1285.7 mW cm^{-3}	72 % (1000)	[220]
(Cu,Co)Se_2 Nanocubes and Ti-MXene	Screen printing	DI water	10 Pa s at 100 S^{-1}	PVA/KOH	(IDE) (1.0 V)	58 mF cm^{-2} at 1 mA cm^{-2}	8.06 μWh cm^{-2}/5 mW cm^{-2}	84 % (10000)	[221]

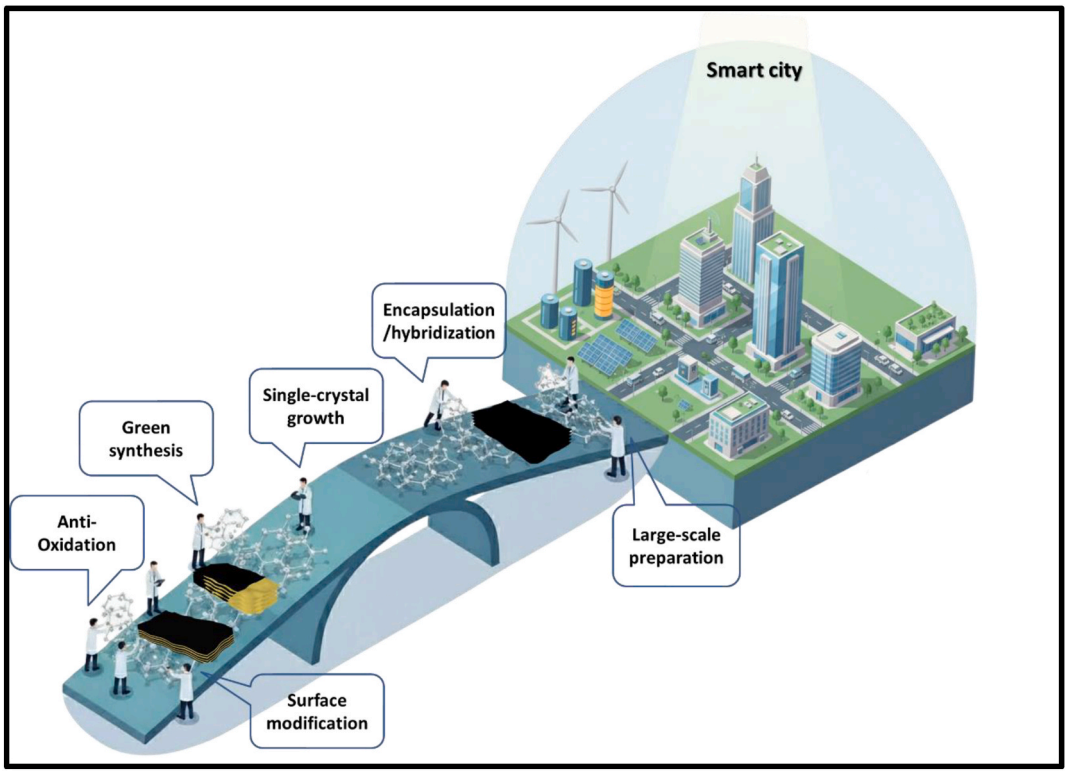

Fig. 13. The upcoming challenges and directions for the $Ti_3C_2T_x$ MXene-based composites.

MXenes for energy applications will be significantly advanced.

CRediT authorship contribution statement

Naveen Kumar: Writing – review & editing, Writing – original draft. **Quy-Van Hoang:** Methodology, Conceptualization. **Mohamed Ahmed Belal:** Writing – review & editing, Writing – original draft. **Kushal Ruthvik Kaja:** Writing – review & editing, Writing – original draft. **Phi Hung Nguyen:** Writing – review & editing, Writing – original draft. **Quynh Le-Van:** Writing – review & editing, Writing – original draft. **Vien Vo:** Writing – review & editing, Writing – original draft. **Vo Thi Thuy Linh:** Writing – review & editing, Writing – original draft. **Phan Khanh Thinh Nguyen:** Writing – review & editing, Writing – original draft. **Qui Thanh Hoai Ta:** Writing – review & editing, Writing – original draft.

Declaration of competing interest

The authors declare that they have no competing financial interests or personal relationships that could have influenced the work reported in this study.

Acknowledgments

This work was funded by the Vietnam Academy of Science and Technology (VAST) under Grant Number THTEXS.02/24-26.

References

[1] C. Nie, C. Lin, B. Li, F. Chen, H. Guo, J. Li, L. Liang, Y. Wang, Y. Wu, H. Zheng, A novel E-Sticker based on triboelectric nanogenerators for wireless passive communication, Adv. Funct. Mater. (2025) 2425965, https://doi.org/10.1002/ADFM.202425965.

[2] B. Mikaeeli Kangarshahi, S.M. Naghib, D. Younesian, N. Rabiee, Unlocking the rhythmic power of bacterial cellulose: a comprehensive review on green energy harvesting and sustainable applications, Adv. Funct. Mater. 35 (2025) 2413760, https://doi.org/10.1002/ADFM.202413760.

[3] M.N. Tran, A. Skorynina, A. Addad, A. Fadel, K. Ben Tayeb, L. Karmazin, L. Thomas, M. Corda, Y. Wisse, O. Vovk, A.Y. Khodakov, B. Grandidier, V. Ordomsky, Electricity-driven selectivity in the photocatalytic oxidation of methane to carbon monoxide with liquid gallium-semiconductor composite, Appl. Catal. B Environ. Energy 363 (2025) 124834, https://doi.org/10.1016/J.APCATB.2024.124834.

[4] M.N. Tran, M. Moreau, A. Addad, A. Teurtrie, T. Roland, V. de Waele, M. Dewitte, L. Thomas, G. Levêque, C. Dong, Boosting gas-phase TiO2 photocatalysis with weak electric field strengths of Volt/Centimeter, ACS Appl. Mater. Interfaces 16 (2024) 14852–14863.

[5] W.M. Rumaherang, H.I. Elim, A. Latununuwe, E.K. Huliselan, J.D. Lekalette, Performance energy production with advanced design and prototype floating ducted tidal turbine for small islands, Renew. Sustain. Energy Rev. 216 (2025) 115664, https://doi.org/10.1016/J.RSER.2025.115664.

[6] Y. Zhu, T. Liu, L. Sun, C. Song, Combined tidal power system with pumped storage function, J. Energy Storage 117 (2025) 116119, https://doi.org/10.1016/J.EST.2025.116119.

[7] E.R. Zvereva, G.E. Marin, I.G. Akhmetova, L.O. Zverev, Prospects for obtaining green hydrogen at mini-hydroelectric power plants for transport, Int. J. Hydrogen Energy 97 (2025) 291–298, https://doi.org/10.1016/J.IJHYDENE.2024.11.308.

[8] A. Kumar, D.B. Pal, Renewable Energy Development Sources and Technology: Overview, 2025, pp. 1–23, https://doi.org/10.1007/978-981-97-9626-7_1.

[9] S. Gupta, J.J. Zhang, J. Lei, H. Yu, M. Liu, X. Zou, B.I. Yakobson, Two-Dimensional transition metal dichalcogenides: a theory and simulation perspective, Chem. Rev. 125 (2025) 786–834, https://doi.org/10.1021/ACS.CHEMREV.4C00628.

[10] B. Zhang, T. Su, C. Rong, T. Yu, S. Hu, P. He, Y. Yan, F. Xuan, Progress and perspectives of high-quality mechanical properties testing and mechanisms for 2D materials, Int. J. Extrem. Manuf. (2025), https://doi.org/10.1088/2631-7990/AE0216.

[11] Z. Lin, X. Yang, J. He, N. Dong, B. Li, Structural and optoelectronic characterization of anisotropic two-dimensional materials and applications in polarization-sensitive photodetectors, Appl. Phys. Rev. 12 (2025), https://doi.org/10.1063/5.0226193.

[12] P.T. Phan, Q.T.H. Ta, P.K.T. Nguyen, Designed synthesis of three-dimensional covalent organic frameworks: a mini review, Polymers 15 (2023) 887, https://doi.org/10.3390/POLYM15040887, 15 (2023) 887.

[13] Q.T.H. Ta, D. Thakur, J.S. Noh, Design of functional Ti3C2Tx MXene for gas sensors and energy harvesting: a review, Chemosensors 11 (2023) 477, https://doi.org/10.3390/CHEMOSENSORS11090477, 11 (2023) 477.

[14] A. Saxena, A. Tyagi, S. Vats, I. Gupta, A. Gupta, R. Kaur, S.K. Tiwary, A. A. Elzatahry, M. Singh, A. Karim, MXene-Integrated composites for biomedical applications: synthesis, cancer diagnosis, and emerging frontiers, Small Science 5 (2025) 2400492, https://doi.org/10.1002/SMSC.202400492.

[15] Y. Sun, W. He, C. Jiang, J. Li, J. Liu, M. Liu, Wearable biodevices based on two-dimensional materials: from flexible sensors to smart integrated systems, Nano-

Micro Lett. 17 (2025) 1–49, https://doi.org/10.1007/S40820-024-01597-W, 2025 17:1.
[16] A. Kamal, B. Li, A. Solayman, S. Luo, I. Kinloch, L. Zheng, K. Liao, Mechanical properties of two-dimensional material-based thin films: a comprehensive review, Nanoscale Horiz 10 (2025) 512–536, https://doi.org/10.1039/D4NH00425F.
[17] S. Supriya, S. Senapati, R. Naik, 2D chalcogenide heterostructures: a discussion on its synthesis, properties and emerging applications, Next Mater. 7 (2025) 100368, https://doi.org/10.1016/J.NXMATE.2024.100368.
[18] M. Naguib, M. Kurtoglu, V. Presser, J. Lu, J. Niu, M. Heon, L. Hultman, Y. Gogotsi, M.W. Barsoum, Two-dimensional nanocrystals produced by exfoliation of Ti3AlC2, Adv. Mater. 23 (2011) 4248–4253.
[19] Y. Gogotsi, Mxenes: from Discovery to Applications of Two-Dimensional Metal Carbides and Nitrides, CRC Press, 2023.
[20] B. Xu, Y. Gogotsi, MXenes: from discovery to applications, Adv. Funct. Mater. 30 (2020).
[21] K. Hantanasirisakul, Y. Gogotsi, Electronic and optical properties of 2D transition metal carbides and nitrides (MXenes), Adv. Mater. 30 (2018) 1804779.
[22] B. Anasori, Y. Gogotsi, The Global Expansion of Mxenes, Graphene and 2D Materials, 2023, pp. 1–3.
[23] M.W. Barsoum, Y. Gogotsi, Removing roadblocks and opening new opportunities for MXenes, Ceram. Int. 49 (2023) 24112–24122.
[24] C.E. Shuck, Y. Gogotsi, Beyond Single-M Mxenes, Transition Metal Carbides and Nitrides (Mxenes) Handbook: Synthesis, Processing, Properties and Applications, 2024, pp. 189–213, https://doi.org/10.1002/9781119869528.CH9.
[25] M. Naguib, M.W. Barsoum, Y. Gogotsi, Ten years of progress in the synthesis and development of MXenes, Adv. Mater. 33 (2021) 2103393.
[26] A.V. Mohammadi, J. Rosen, Y. Gogotsi, The world of two-dimensional carbides and nitrides (MXenes), Science 372 (2021) (1979), https://doi.org/10.1126/science.abf1581.
[27] B. Anasori, M.R. Lukatskaya, Y. Gogotsi, 2D metal carbides and nitrides (MXenes) for energy storage. https://doi.org/10.1038/natrevmats.2016.98, 2017.
[28] B. Anasori, M.R. Lukatskaya, Y. Gogotsi, 2D metal carbides and nitrides (MXenes) for energy storage, Nat. Rev. Mater. 2 (2017) 16098, https://doi.org/10.1038/natrevmats.2016.98.
[29] X. Xiao, H. Wang, P. Urbankowski, Y. Gogotsi, Topochemical synthesis of 2D materials, Chem. Soc. Rev. 47 (2018) 8744–8765, https://doi.org/10.1039/c8cs00649k.
[30] V.N. Borysiuk, V.N. Mochalin, Y. Gogotsi, Molecular dynamic study of the mechanical properties of two-dimensional titanium carbides Tin+1Cn (MXenes), Nanotechnology 26 (2015) 265705, https://doi.org/10.1088/0957-4484/26/26/265705.
[31] M. Downes, C.E. Shuck, B. McBride, J. Busa, Y. Gogotsi, Comprehensive synthesis of Ti3C2T x from MAX phase to MXene, Nat. Protoc. (2024) 1–28.
[32] A. Iqbal, T. Hassan, S.M. Naqvi, Y. Gogotsi, C.M. Koo, MXenes for multispectral electromagnetic shielding, Nat. Rev. Electr. Eng. 1 (2024) 180–198.
[33] L. Fei, L. Lei, H. Xu, X. Guo, B. Chen, X. Han, X. Chen, Q. Huang, D. Wang, Ion transport behaviors in MXenes for electrochemical energy storage and conversion, Carbon Energy 7 (2025) e678, https://doi.org/10.1002/CEY2.678.
[34] D. Jayan, R. Ramdas, Electronic, electrical and optical properties of MXenes, MXene reinforced polymer composites: fabrication, Characterization and Applications (2024) 107–145, https://doi.org/10.1002/9781119901280.CH4.
[35] K. Khan, A.K. Tareen, W. Ahmad, I. Hussain, M.U. Chaudhry, A. Mahmood, M. F. Khan, H. Zhang, Z. Xie, Recent advances in Non-Ti MXenes: synthesis, properties, and novel applications, Adv. Sci. 11 (2024) 2303998, https://doi.org/10.1002/ADVS.202303998.
[36] K. Deshmukh, A. Muzaffar, T. Kovárík, M.B. Ahamed, S.K.K. Pasha, Introduction to 2D MXenes: fundamental aspects, MAX phases and MXene derivatives, current challenges, and future prospects, MXenes and Their Composites: Synthesis, Properties and Potential Applications (2022) 1–47, https://doi.org/10.1016/B978-0-12-823361-0.00009-5.
[37] M. Ghidiu, M.R. Lukatskaya, M.-Q. Zhao, Y. Gogotsi, M.W. Barsoum, Conductive two-dimensional titanium carbide 'clay' with high volumetric capacitance, Nature 516 (2014) 78–81.
[38] L. Han, Y. Li, C. Chen, L. Liu, Z. Lu, Multifunctional enhanced energy density of flexible wide-temperature supercapacitors based on MXene/PANI conductive hydrogel, Chem. Eng. J. 485 (2024) 149951, https://doi.org/10.1016/J.CEJ.2024.149951.
[39] J. FitzPatrick, S. Bera, A. Inman, A. Cabrera, T. Zhang, T. Parker, B. S. Mohammadlou, I. Roslyk, S. Ippolito, K. Shevchuk, S.A. Kadam, N.R. Pradhan, Y. Gogotsi, Record efficiency of β-Phase PVDF-MXene composites in thin-film dielectric capacitors, Adv. Mater. 37 (2025) 2419088, https://doi.org/10.1002/ADMA.202419088.
[40] R. Raveendrakurup, A.T. Prasannakumar, R.R. Mohan, J. Cherusseri, S.J. Varma, Supercapacitors: fundamentals, working principle, classifications, energy storage mechanisms, nanostructured electrode and electrolyte materials, promises, challenges, and future perspectives, Nanostructured Materials for Energy Storage (2024) 821–858, https://doi.org/10.1002/9783527838851.CH23.
[41] Y.K. Sharma, Y. Kumar, S. Sharma, M. Gupta, Nanotechnologies in the renewable energy sector, Renewable Energy Innovations (2024) 41–82, https://doi.org/10.1002/9781119785712.CH2.
[42] J. He, J.D. Butson, R. Gu, A.C.M. Loy, Q. Fan, L. Qu, G.K. Li, Q. Gu, MXene-Supported single-atom electrocatalysts, Adv. Sci. (2025) 2414674, https://doi.org/10.1002/ADVS.202414674.
[43] E. Kotob, M.M. Awad, M. Umar, O.A. Taialla, I. Hussain, S.I. Alsabbahen, K. Alhooshani, S.A. Ganiyu, Unlocking CO2 conversion potential with single atom catalysts and machine learning in energy application, iScience 0 (2025) 112306, https://doi.org/10.1016/J.ISCI.2025.112306.
[44] Z. Lei, S. Ali, C.I. Sathish, M.I. Ahmed, J. Qu, R. Zheng, S. Xi, X. Yu, M.B. H. Breese, C. Liu, J. Zhang, S. Qi, X. Guan, V. Perumalsamy, M. Fawaz, J.H. Yang, M. Bououdina, K. Domen, A. Vinu, L. Qiao, J. Yi, Transition metal carbonitride MXenes anchored with Pt sub-nanometer clusters to achieve high-performance hydrogen evolution reaction at all pH range, Nano-Micro Lett. 17 (2025) 1–15, https://doi.org/10.1007/S40820-025-01654-Y/FIGURES/5.
[45] Q.T. Hoai Ta, M. Jianbin, N. Thi Chau, N. Hoi Nguyen, D. Linh Tran, T.M. Huyen Nguyen, M. Hoang Tran, Van-Quy Hoang, Soonmin Seo, D. Hai Nguyen, Recent progress in the synthesis of nanostructured Ti3C2Tx MXene for energy storage and wastewater treatment: a review, Nanoscale Adv. 24 (2025) 49, https://doi.org/10.1039/D5NA00021A.
[46] Q.T.H. Ta, L.T. Nhiem, D.T.Y. Oanh, N.H. Hieu, P.K.T. Nguyen, Review on progress in synthesis of CdS-based composites and their potential applications, Vietnam Journal of Chemistry (2024), https://doi.org/10.1002/VJCH.202400155.
[47] A. Sreedhar, P. Ravi, J.-S. Noh, Advancements in two-dimensional Ti3C2 MXene interfaced semiconductors for room temperature NO2 gas sensing: a review, J. Mater. Sci. Technol. 203 (2024) 237–254.
[48] P.V. Vaishag, J.S. Noh, A comparative review of graphene and MXene-Based composites towards gas sensing, Molecules 29 (2024) 4558, https://doi.org/10.3390/MOLECULES29194558, 29 (2024) 4558.
[49] T. Ramachandran, R.K. Raji, M. Rezeq, From lab to market: the future of zinc–air batteries powered by MOF/MXene hybrids, J Mater Chem A Mater 13 (2025) 12855–12890, https://doi.org/10.1039/D5TA01344E.
[50] S. Bashir, L. Gurbanova, I.A. Shaaban, M.S. Javed, M.R. Karim, S.S.A. Shah, M. A. Nazir, Recent advances in MXene-polymer composites for high performance supercapacitor applications, J. Energy Storage 132 (2025) 117588, https://doi.org/10.1016/J.EST.2025.117588.
[51] M. Misra, A. Sreedhar, J.S. Noh, Advancements in 2D Ti3C2 MXene interfaced various metal oxide semiconductors for photoelectrochemical water splitting: a review, Microchem. J. 216 (2025) 114632, https://doi.org/10.1016/J.MICROC.2025.114632.
[52] P.V. Vaishag, Y.H. Bae, J.S. Noh, PMMA microspheres-embedded Ti3C2Tx MXene heterophotocatalysts synergistically working for multiple dye degradation, J. Ind. Eng. Chem. 140 (2024) 490–500, https://doi.org/10.1016/J.JIEC.2024.06.006.
[53] Y.A. Kumar, T. Ramachandran, A. Ghosh, A.G. Al-Sehemi, N.P. Reddy, M. Moniruzzaman, A review on in-plane ordered MXenes-based materials in addressing challenges faced by biosensor applications, J. Energy Storage 121 (2025) 116507, https://doi.org/10.1016/J.EST.2025.116507.
[54] T. Ramachandran, F. Hamed, Y.A. Kumar, R.K. Raji, H.H. Hegazy, Multifunctional covalent-organic frameworks (COFs)-2D MXenes composites for diverse applications, J. Energy Storage 73 (2023) 109299, https://doi.org/10.1016/J.EST.2023.109299.
[55] T. Ramachandran, R.M.N. Kalla, A.G. Al-Sehemi, Y.A. Kumar, R. Khan, A. Ghosh, S.S. Rao, J. Lee, Beyond traditional MXenes: the promise of non-Ti MXenes in energy and catalysis, Colloids Surf. A Physicochem. Eng. Asp. 726 (2025) 137844, https://doi.org/10.1016/J.COLSURFA.2025.137844.
[56] Q.T.H. Ta, N.M. Tran, N.N. Tri, A. Sreedhar, J.S. Noh, Highly surface-active Si-doped TiO2/Ti3C2Tx heterostructure for gas sensing and photodegradation of toxic matters, Chem. Eng. J. 425 (2021) 131437, https://doi.org/10.1016/j.cej.2021.131437.
[57] L.T. Nhiem, J. Mao, Q.T. Hoai Ta, S. Seo, Highly selective ethanol gas sensor based on CdS/Ti 3 C 2 T x MXene composites, Nanoscale Adv. 7 (2025) 1452–1463, https://doi.org/10.1039/D4NA00927D.
[58] Q.T.H. Ta, N.N. Tri, J.-S. Noh, Improved NO2 gas sensing performance of 2D MoS2/Ti3C2Tx MXene nanocomposite, Appl. Surf. Sci. (2022) 154624.
[59] Q.T.H. Ta, A. Sreedhar, N.N. Tri, J.-S. Noh, In situ growth of TiO2 on Ti3C2Tx MXene for improved gas-sensing performances, Ceram. Int.50 (2024) 27227–27236.
[60] M. Yadav, M. Kumar, A. Sharma, Review of Ti3C2Tx MXene nanosheets and their applications, ACS Appl. Nano Mater. 7 (2024) 9847–9867, https://doi.org/10.1021/ACSANM.4C00316/ASSET/IMAGES/MEDIUM/AN4C00316_0011.GIF.
[61] A. Kagalkar, S. Dharaskar, N. Chaudhari, 2D-Transition metal carbides and nitrides: prospects and challenges, ACS (Am. Chem. Soc.) Symp. Ser. 1445 (2023) 1–42, https://doi.org/10.1021/BK-2023-1445.CH001.
[62] N. Khatun, Progresses and challenges in 2D MXenes: synthesis, Intercalation/Delamination, and storage, ACS (Am. Chem. Soc.) Symp. Ser. 1442 (2023) 101–141, https://doi.org/10.1021/BK-2023-1442.CH005.
[63] M. Alhabeb, K. Maleski, B. Anasori, P. Lelyukh, L. Clark, S. Sin, Guidelines for synthesis and processing of two-dimensional titanium Carbide (Ti3C2Tx MXene). https://doi.org/10.1021/acs.chemmater.7b02847, 2017.
[64] N.M. Tran, Q.T.H. Ta, A. Sreedhar, J.-S. Noh, Ti3C2Tx MXene playing as a strong methylene blue adsorbent in wastewater, Appl. Surf. Sci. 537 (2021) 148006.
[65] Y. Li, H. Shao, Z. Lin, J. Lu, L. Liu, B. Duployer, P.O.Å. Persson, P. Eklund, L. Hultman, M. Li, K. Chen, X.H. Zha, S. Du, P. Rozier, Z. Chai, E. Raymundo-Piñero, P.L. Taberna, P. Simon, Q. Huang, A general Lewis acidic etching route for preparing MXenes with enhanced electrochemical performance in non-aqueous electrolyte, Nat. Mater. 19 (2020) 894–899, https://doi.org/10.1038/S41563-020-0657-0. TECHMETA.
[66] A. Jawaid, A. Hassan, G. Neher, D. Nepal, R. Pachter, W.J. Kennedy, S. Ramakrishnan, R.A. Vaia, Halogen etch of Ti3AlC2 MAX phase for MXene fabrication, ACS Nano 15 (2021) 2771–2777.
[67] T. Li, L. Yao, Q. Liu, J. Gu, R. Luo, J. Li, X. Yan, W. Wang, P. Liu, B. Chen, W. Zhang, W. Abbas, R. Naz, D. Zhang, Fluorine-Free synthesis of high-purity

Ti3C2Tx (T=OH, O) via Alkali treatment, Angew. Chem. Int. Ed. 57 (2018) 6115–6119, https://doi.org/10.1002/ANIE.201800887.
[68] S. Yang, P. Zhang, F. Wang, A.G. Ricciardulli, M.R. Lohe, P.W.M. Blom, X. Feng, Fluoride-free synthesis of two-dimensional titanium carbide (MXene) using a binary aqueous system, Angew. Chem. 130 (2018) 15717–15721.
[69] Y. Wang, J. Li, W. Han, C. Zhao, S. Xu, D. Wang, Z. Yu, M. Lu, H. Li, M. Zhang, Multi-ion competition mechanism within MXene interlayer and Li ion intercalated electrode function, Appl. Surf. Sci. 623 (2023) 157043, https://doi.org/10.1016/J.APSUSC.2023.157043.
[70] R. Mangiri, T. Ramachandran, Y.A. Kumar, A. Ghosh, A.G. Al-Sehemi, A.K. Yadav, D. Mani, Surface engineering of M5X4 MXenes for next-gen energy solutions, Mater. Today Chem. 48 (2025) 102864, https://doi.org/10.1016/J.MTCHEM.2025.102864.
[71] K. Roy, N. Rani M, M.P. Narayanaswamy, T. Sardar, S. Vidyashankar, D. Rangappa, Rapid and direct conversion of the Ti3AlC2 MAX phase to Ti3C2Tx MXene nanosheets by a supercritical water-assisted etching process, ACS Appl. Nano Mater. 7 (2024) 27628–27639, https://doi.org/10.1021/ACSANM.4C05612.
[72] N.M. Tran, Q.T.H. Ta, J.-S. Noh, Unusual synthesis of safflower-shaped TiO2/Ti3C2 heterostructures initiated from two-dimensional Ti3C2 MXene, Appl. Surf. Sci. 538 (2021) 148023.
[73] T. Li, L. Yao, Q. Liu, J. Gu, R. Luo, J. Li, X. Yan, W. Wang, P. Liu, B. Chen, Fluorine-free synthesis of high-purity Ti3C2Tx (T= OH, O) via alkali treatment, Angew. Chem. Int. Ed. 57 (2018) 6115–6119.
[74] J. Pang, R.G. Mendes, A. Bachmatiuk, L. Zhao, H.Q. Ta, T. Gemming, H. Liu, Z. Liu, M.H. Rummeli, Applications of 2D MXenes in energy conversion and storage systems, Chem. Soc. Rev. 48 (2019) 72–133, https://doi.org/10.1039/C8CS00324F.
[75] H.W. Wang, M. Naguib, K. Page, D.J. Wesolowski, Y. Gogotsi, Resolving the structure of Ti3C2Tx MXenes through multilevel structural modeling of the atomic pair distribution function, Chem. Mater. 28 (2016) 349–359, https://doi.org/10.1021/ACS.CHEMMATER.5B04250/SUPPL_FILE/CM5B04250_SI_001.PDF.
[76] A.N. Enyashin, A.L. Ivanovskii, Structural and electronic properties and stability of MX enes Ti 2C and Ti3C2 functionalized by methoxy groups, J. Phys. Chem. C 117 (2013) 13637–13643, https://doi.org/10.1021/JP401820B/ASSET/IMAGES/MEDIUM/JP-2013-01820B_0005.GIF.
[77] Y. Xie, M. Naguib, V.N. Mochalin, M.W. Barsoum, Y. Gogotsi, X. Yu, K.W. Nam, X. Q. Yang, A.I. Kolesnikov, P.R.C. Kent, Role of surface structure on Li-ion energy storage capacity of two-dimensional transition-metal carbides, J. Am. Chem. Soc. 136 (2014) 6385–6394, https://doi.org/10.1021/JA501520B.
[78] M. Naguib, V.N. Mochalin, M.W. Barsoum, Y. Gogotsi, M. Naguib, V.N. Mochalin, M.W. Barsoum, Y. Gogotsi, 25th anniversary article: mxenes: a new family of two-dimensional materials, Adv. Mater. 26 (2014) 992–1005, https://doi.org/10.1002/ADMA.201304138.
[79] A. Lipatov, A. Sinitskii, Electronic and Mechanical Properties of Mxenes Derived from Single-Flake Measurements, 2D Metal Carbides and Nitrides (Mxenes): Structure, Properties and Applications, 2019, pp. 301–325, https://doi.org/10.1007/978-3-030-19026-2_16.
[80] C. Rong, T. Su, Z. Li, T. Chu, M. Zhu, Y. Yan, B. Zhang, F.Z. Xuan, Elastic properties and tensile strength of 2D Ti3C2Tx MXene monolayers, Nat. Commun. 15 (2024) 1–8, https://doi.org/10.1038/S41467-024-45657-6. TECHMETA.
[81] K. Hantanasirisakul, M.Q. Zhao, P. Urbankowski, J. Halim, B. Anasori, S. Kota, C. E. Ren, M.W. Barsoum, Y. Gogotsi, Fabrication of Ti3C2Tx MXene transparent thin films with tunable optoelectronic properties, Adv Electron Mater 2 (2016) 1600050, https://doi.org/10.1002/AELM.201600050.
[82] A. Ali, A. Belaidi, S. Ali, M.I. Helal, K.A. Mahmoud, Transparent and conductive Ti3C2Tx (MXene) thin film fabrication by electrohydrodynamic atomization technique, J. Mater. Sci. Mater. Electron. 27 (2016) 5440–5445, https://doi.org/10.1007/S10854-016-4447-Z/METRICS.
[83] D. Xiong, X. Li, Z. Bai, S. Lu, Recent advances in layered Ti3C2Tx MXene for electrochemical energy storage, Small 14 (2018) 1703419.
[84] X. Wang, X. Shen, Y. Gao, Z. Wang, R. Yu, L. Chen, Atomic-scale recognition of surface structure and intercalation mechanism of Ti3C2X, J. Am. Chem. Soc. 137 (2015) 2715–2721, https://doi.org/10.1021/JA512820K/SUPPL_FILE/JA512820K_SI_001.PDF.
[85] N.R. Hemanth, B. Kandasubramanian, Recent advances in 2D MXenes for enhanced cation intercalation in energy harvesting applications: a review, Chem. Eng. J. 392 (2020) 123678, https://doi.org/10.1016/J.CEJ.2019.123678.
[86] B. Akuzum, K. Maleski, B. Anasori, P. Lelyukh, N.J. Alvarez, E.C. Kumbur, Y. Gogotsi, Rheological characteristics of 2D Titanium Carbide (MXene) dispersions: a guide for processing MXenes, ACS Nano 12 (2018) 2685–2694, https://doi.org/10.1021/ACSNANO.7B08889.
[87] M. Greaves, M. Mende, J. Wang, W. Yang, S. Barg, Investigating the rheology of 2D titanium carbide (MXene) dispersions for colloidal processing: progress and challenges, J. Mater. Res. 36 (2021) 4578–4600, https://doi.org/10.1557/S43578-021-00282-7/FIGURES/13.
[88] B. Ahmed, D.H. Anjum, M.N. Hedhili, Y. Gogotsi, H.N. Alshareef, H2O2 assisted room temperature oxidation of Ti2C MXene for Li-ion battery anodes, Nanoscale 8 (2016) 7580–7587, https://doi.org/10.1039/C6NR00002A.
[89] On the Structural Stability of Mxene and the Role of Transition Metal Adatoms - Nanoscale (RSC Publishing) DOI:10.1039/C8NR01986J, (n.d.). https://pubs.rsc.org/en/content/articlehtml/2018/nr/c8nr01986j (accessed October 1, 2025).
[90] H. Wang, Y. Wu, J. Zhang, G. Li, H. Huang, X. Zhang, Q. Jiang, Enhancement of the electrical properties of MXene Ti3C2 nanosheets by post-treatments of alkalization and calcination, Mater. Lett. 160 (2015) 537–540, https://doi.org/10.1016/J.MATLET.2015.08.046.
[91] Z. Li, L. Wang, D. Sun, Y. Zhang, B. Liu, Q. Hu, A. Zhou, Synthesis and thermal stability of two-dimensional carbide MXene Ti3C2, Mater. Sci. Eng., B 191 (2015) 33–40, https://doi.org/10.1016/J.MSEB.2014.10.009.
[92] Y. Wen, T.E. Rufford, X. Chen, N. Li, M. Lyu, L. Dai, L. Wang, Nitrogen-doped Ti3C2Tx MXene electrodes for high-performance supercapacitors, Nano Energy 38 (2017) 368–376.
[93] J. Zhang, N. Kong, D. Hegh, K.A.S. Usman, G. Guan, S. Qin, I. Jurewicz, W. Yang, J.M. Razal, Freezing Titanium carbide aqueous dispersions for ultra-long-term storage, ACS Appl. Mater. Interfaces 12 (2020) 34032–34040, https://doi.org/10.1021/ACSAMI.0C06728.
[94] T. Habib, X. Zhao, S.A. Shah, Y. Chen, W. Sun, H. An, J.L. Lutkenhaus, M. Radovic, M.J. Green, Oxidation stability of Ti3C2Tx MXene nanosheets in solvents and composite films, NPJ 2D Mater Appl 3 (2019) 1–6, https://doi.org/10.1038/S41699-019-0089-3;SUBJMETA=1018,301,357,551,639;KWRD=SYNTHESIS+AND+PROCESSING,TWO-DIMENSIONAL+MATERIALS.
[95] An Investigation into the Factors Governing the Oxidation of two-dimensional Ti 3 C 2 Mxene - Nanoscale (RSC Publishing) DOI:10.1039/C9NR00084D, (n.d.). https://pubs.rsc.org/en/content/articlehtml/2019/nr/c9nr00084d?casa_token=Oc2n7hggWe8AAAAA:J8MkGR1YStbm4N7KyFwJ7ECditswaELmQtHvdXGyN9ZHlKCsqLuPTGtLVWQo_P2s5mLtSPy0oQ1sqO4 (accessed October 2, 2025).
[96] J. Zhang, S. Seyedin, S. Qin, Z. Wang, S. Moradi, F. Yang, P.A. Lynch, W. Yang, J. Liu, X. Wang, J.M. Razal, Highly conductive Ti3C2Tx MXene hybrid fibers for flexible and elastic fiber-shaped supercapacitors, Small 15 (2019) 1804732, https://doi.org/10.1002/SMLL.201804732.
[97] C. Gao, Y. Zhang, Z. Yang, C. Liu, J. Chen, Q. Gao, Green synthesis of continuous wet-spun PEDOT: pss/mxene composite fibers for highly efficient microsupercapacitors, ACS Appl. Energy Mater. 8 (2025) 5230–5238, https://doi.org/10.1021/ACSAEM.5C00180.
[98] T.Y. Ko, D. Kim, S.J. Kim, H. Kim, A.S. Nissimagoudar, S.C. Lee, X. Lin, P. T. Cummings, S. Doo, S. Park, T. Hassan, T. Oh, A. Chae, J. Lee, Y. Gogotsi, I. In, C.M. Koo, Universal ligands for dispersion of two-dimensional MXene in organic solvents, ACS Nano 17 (2023) 1112–1119, https://doi.org/10.1021/ACSNANO.2C08209/SUPPL_FILE/NN2C08209_SI_008.MP4.
[99] T.Y. Ko, H. Ye, G. Murali, S.Y. Lee, Y.H. Park, J. Lee, J. Lee, D.J. Yun, Y. Gogotsi, S.J. Kim, S.H. Kim, Y.J. Jeong, S.J. Park, I. In, Functionalized MXene ink enables environmentally stable printed electronics, Nat. Commun. 15 (2024) 1–12, https://doi.org/10.1038/S41467-024-47700-Y. TECHMETA.
[100] T. Ramachandran, R.K. Raji, S. Palanisamy, N. Renuka, K. Karuppasamy, The role of in situ and operando techniques in unraveling local electrochemical supercapacitor phenomena, J. Ind. Eng. Chem. 145 (2025) 144–168, https://doi.org/10.1016/J.JIEC.2024.10.077.
[101] S. Doo, A. Chae, D. Kim, T. Oh, T.Y. Ko, S.J. Kim, D.Y. Koh, C.M. Koo, Mechanism and kinetics of oxidation reaction of aqueous Ti3C2Tx suspensions at different pHs and temperatures, ACS Appl. Mater. Interfaces 13 (2021) 22855–22865, https://doi.org/10.1021/ACSAMI.1C04663.
[102] M.S. Alam, M.A. Chowdhury, M.A. Kowser, M.S. Islam, M.M. Islam, T. Khandaker, Advances of MAX phases: synthesis, characterizations and challenges, Eng. Rep. 6 (2024) e12911, https://doi.org/10.1002/ENG2.12911.
[103] T.S. Mathis, K. Maleski, A. Goad, A. Sarycheva, M. Anayee, A.C. Foucher, K. Hantanasirisakul, C.E. Shuck, E.A. Stach, Y. Gogotsi, Modified MAX phase synthesis for environmentally stable and highly conductive Ti3C2 MXene, ACS Nano 15 (2021) 6420–6429, https://doi.org/10.1021/ACSNANO.0C08357.
[104] Y. Yang, Z. Cao, L. Shi, R. Wang, J. Sun, Enhancing the conductivity, stability and flexibility of Ti3C2Tx MXenes by regulating etching conditions, Appl. Surf. Sci. 533 (2020) 147475, https://doi.org/10.1016/J.APSUSC.2020.147475.
[105] Shaista Nouseen, Martin Pumera, Electrochemical etching of MXenes: mechanism, challenges and future outlooks, J Mater Chem A Mater (2025), https://doi.org/10.1039/D5TA04176G.
[106] C.J. Zhang, S. Pinilla, N. McEvoy, C.P. Cullen, B. Anasori, E. Long, S.H. Park, A. Seral-Ascaso, A. Shmeliov, D. Krishnan, C. Morant, X. Liu, G.S. Duesberg, Y. Gogotsi, V. Nicolosi, Oxidation stability of colloidal two-dimensional titanium carbides (MXenes), Chem. Mater. 29 (2017) 4848–4856, https://doi.org/10.1021/ACS.CHEMMATER.7B00745/SUPPL_FILE/CM7B00745_SI_002.AVI.
[107] X. Zhang, X. Liu, Y. Feng, S. Qiu, M. Lu, P. Bo, Q. Liao, Y. Liu, H. Li, Stabilizing the MXene by ion confinement shielding in a wide temperature range, Small Struct. 4 (2023) 2200309, https://doi.org/10.1002/SSTR.202200309.
[108] W.Y. Chen, S.N. Lai, C.C. Yen, X. Jiang, D. Peroulis, L.A. Stanciu, Surface functionalization of Ti3C2Tx MXene with highly reliable superhydrophobic protection for volatile organic compounds sensing, ACS Nano 14 (2020) 11490–11501, https://doi.org/10.1021/ACSNANO.0C03896.
[109] X.Y. Wang, S.Y. Liao, H.P. Huang, Q.F. Wang, Y.Y. Shi, P.L. Zhu, Y.G. Hu, R. Sun, Y.J. Wan, Enhancing the chemical stability of MXene through synergy of hydrogen bond and coordination bond in aqueous solution, Small Methods 7 (2023) 2201694, https://doi.org/10.1002/SMTD.202201694.
[110] X. Zhao, D.E. Holta, Z. Tan, J.H. Oh, I.J. Echols, M. Anas, H. Cao, J.L. Lutkenhaus, M. Radovic, M.J. Green, Annealed Ti3C2Tz MXene films for oxidation-resistant functional coatings, ACS Appl. Nano Mater. 3 (2020) 10578–10585, https://doi.org/10.1021/ACSANM.0C02473.
[111] N. Liu, Q. Li, H. Wan, L. Chang, H. Wang, J. Fang, T. Ding, Q. Wen, L. Zhou, X. Xiao, High-temperature stability in air of Ti3C2Tx MXene-based composite with extracted bentonite, Nat. Commun. 13 (2022) 1–10, https://doi.org/10.1038/S41467-022-33280-2. TECHMETA.

[112] C. Roy, S.K. De, P. Banerjee, S. Pradhan, S. Bhattacharyya, Investigating suitable medium for the long-duration storage of Ti2CTx MXene, J. Alloys Compd. 938 (2023) 168471, https://doi.org/10.1016/J.JALLCOM.2022.168471.
[113] Z. Bo, R. Wang, B. Wang, S. Sunny, Y. Zhao, K. Ge, K. Xu, Y. Song, E. Raymundo-Piñero, Z. Lin, H. Shao, Q. Yu, J. Yan, K. Cen, P.L. Taberna, P. Simon, Ion desolvation for boosting the charge storage performance in Ti3C2 MXene electrode, Nat. Commun. 16 (2025) 1–11, https://doi.org/10.1038/S41467-025-58700-X. TECHMETA.
[114] Y. Ni, X. Zang, J. Chen, T. Zhu, Y. Yang, J. Huang, W. Cai, Y. Lai, Flexible MXene-Based hydrogel enables wearable human–computer interaction for intelligent underwater communication and sensing rescue, Adv. Funct. Mater. 33 (2023) 2301127, https://doi.org/10.1002/ADFM.202301127.
[115] Y. Cui, J. Sun, Y. Wang, L. Zhao, Y. Lv, Y. Tang, W. Zhang, Z. Su, MXene-supported MOF-derived multicore ZrSe2@MnSe2 complex structure for high-rate and long-cycle-life supercapacitors, Fuel 405 (2025) 136630, https://doi.org/10.1016/J.FUEL.2025.136630.
[116] Y. He, Y. Zou, L. Sun, F. Xu, Y. Xia, Y. Chen, S. Wang, Z. Hu, S. Hao, C. Xiang, Multifunctional phase-change materials with Ni-MOF/MXene hierarchical network for thermal energy storage, photothermal conversion, and excellent electromagnetic shielding, J. Energy Storage 119 (2025) 116385, https://doi.org/10.1016/J.EST.2025.116385.
[117] S. Qamar, K. Fatima, N. Ullah, Z. Akhter, A. Waseem, M. Sultan, Recent progress in use of MXene in perovskite solar cells: for interfacial modification, work-function tuning and additive engineering, Nanoscale 14 (2022) 13018–13039, https://doi.org/10.1039/D2NR02799B.
[118] S. Bhattarai, M.K. Hossain, G.F.I. Toki, R. Pandey, J. Madan, D.P. Samajdar, S. Ezzine, L. Ben Farhat, M.Z. Ansari, S.H. Ahammad, A.N.Z. Rashed, Efficiency enhancement of perovskite solar cell devices utilizing MXene and TiO2 as an electron transport layer, New J. Chem. 47 (2023) 17908–17922, https://doi.org/10.1039/D3NJ03548D.
[119] D. Saranin, S. Pescetelli, A. Pazniak, D. Rossi, A. Liedl, A. Yakusheva, L. Luchnikov, D. Podgorny, P. Gostischev, S. Didenko, A. Tameev, D. Lizzit, M. Angelucci, R. Cimino, R. Larciprete, A. Agresti, A. Di Carlo, Transition metal carbides (MXenes) for efficient NiO-based inverted perovskite solar cells, Nano Energy 82 (2021) 105771, https://doi.org/10.1016/J.NANOEN.2021.105771.
[120] Y. Niu, C. Tian, J. Gao, F. Fan, Y. Zhang, Y. Mi, X. Ouyang, L. Li, J. Li, S. Chen, Y. Liu, H.L. Lu, X. Zhao, L. Yang, H. Ju, Y. Yang, C.F. Ding, M. Xu, Q. Xu, Nb2C MXenes modified SnO2 as high quality electron transfer layer for efficient and stability perovskite solar cells, Nano Energy 89 (2021) 106455, https://doi.org/10.1016/J.NANOEN.2021.106455.
[121] L. Yang, D. Kan, C. Dall'Agnese, Y. Dall'Agnese, B. Wang, A.K. Jena, Y. Wei, G. Chen, X.F. Wang, Y. Gogotsi, T. Miyasaka, Performance improvement of MXene-based perovskite solar cells upon property transition from metallic to semiconductive by oxidation of Ti3C2Tx in air, J Mater Chem A Mater 9 (2021) 5016–5025, https://doi.org/10.1039/D0TA11397B.
[122] C. Zhang, W. Li, C. Liu, J. Fan, Y. Mai, Crystallization dependent stability of perovskite solar cells with different hole transporting layers, Sol. RRL 1 (2017) 1700141, https://doi.org/10.1002/SOLR.201700141.
[123] J.H. Heo, F. Zhang, J.K. Park, H. Joon Lee, D.S. Lee, S.J. Heo, J.M. Luther, J. J. Berry, K. Zhu, S.H. Im, Surface engineering with oxidized Ti3C2Tx MXene enables efficient and stable p-i-n-structured CsPbI3 perovskite solar cells, Joule 6 (2022) 1672–1688, https://doi.org/10.1016/J.JOULE.2022.05.013/ATTACHMENT/DF505067-2759-4BBB-AC4A-8E8C2F5DC908/MMC3.PDF.
[124] X. Jin, L. Yang, X.F. Wang, Efficient two-dimensional perovskite solar cells realized by incorporation of Ti3C2Tx MXene as nano-dopants, Nano-Micro Lett. 13 (2021) 1–13, https://doi.org/10.1007/S40820-021-00602-W/FIGURES/6.
[125] L. Yang, Y. Dall'Agnese, K. Hantanasirisakul, C.E. Shuck, K. Maleski, M. Alhabeb, G. Chen, Y. Gao, Y. Sanehira, A.K. Jena, L. Shen, C. Dall'Agnese, X.F. Wang, Y. Gogotsi, T. Miyasaka, SnO2–Ti3C2 MXene electron transport layers for perovskite solar cells, J Mater Chem A Mater 7 (2019) 5635–5642, https://doi.org/10.1039/C8TA12140K.
[126] J.H. Heo, F. Zhang, J.K. Park, H. Joon Lee, D.S. Lee, S.J. Heo, J.M. Luther, J. J. Berry, K. Zhu, S.H. Im, Surface engineering with oxidized Ti3C2Tx MXene enables efficient and stable p-i-n-structured CsPbI3 perovskite solar cells, Joule 6 (2022) 1672–1688, https://doi.org/10.1016/j.joule.2022.05.013.
[127] J. Wang, Z. Cai, D. Lin, K. Chen, L. Zhao, F. Xie, R. Su, W. Xie, P. Liu, R. Zhu, Plasma oxidized Ti3C2Tx MXene as electron transport layer for efficient perovskite solar cells, ACS Appl. Mater. Interfaces 13 (2021) 32495–32502, https://doi.org/10.1021/ACSAMI.1C07146.
[128] Y. Niu, C. Tian, J. Gao, F. Fan, Y. Zhang, Y. Mi, X. Ouyang, L. Li, J. Li, S. Chen, Y. Liu, H.L. Lu, X. Zhao, L. Yang, H. Ju, Y. Yang, C.F. Ding, M. Xu, Q. Xu, Nb2C MXenes modified SnO2 as high quality electron transfer layer for efficient and stability perovskite solar cells, Nano Energy 89 (2021) 106455, https://doi.org/10.1016/J.NANOEN.2021.106455.
[129] X. Liu, H. Tong, Y. Li, W. Li, G. Wan, Q. Liu, Y. Fu, D. He, Z. Li, J. Li, Multifunctional optimization of MXene for enhanced comprehensive performance of Crystal Silicon-MXene back-heterojunction solar cells, Small 21 (2025) 2410160, https://doi.org/10.1002/SMLL.202410160.
[130] N. Ben Ali, R. Agravat, S.K. Patel, A. Armghan, M. Kouki, O.P. Kumar, Optimization of ultra-wideband metamaterial MXene-based polarization-insensitive solar absorber using machine learning for solar heater application, Sci. Rep. 15 (2025) 1–17, https://doi.org/10.1038/s41598-025-93838-0, 2025 15:1.
[131] S.P. Nagalingam, M. Shariq, S. Marimuthu, A.C. Josephine Malathi, S. Pandiaraj, A.N. Alodhayb, A.N. Grace, 2D/2D-Graphene functionalized MXene as an alternative counter electrode for dye-sensitized solar cells, Ind. Eng. Chem. Res. (2024), https://doi.org/10.1021/ACS.IECR.4C01924/SUPPL_FILE/IE4C01924_SI_001.PDF.
[132] M. Rakshita, N. Madathil, A.A. Sharma, P.P. Pradhan, D.P. Durga, U. K. Khanapuram, R.K. Rajaboina, H. Divi, Phosphor-Based triboelectric nanogenerators for mechanical energy harvesting and self-powered systems, ACS Appl. Electron. Mater. 6 (2024) 1821–1828, https://doi.org/10.1021/ACSAELM.3C01728/SUPPL_FILE/EL3C01728_SI_007.MP4.
[133] A. Babu, K. Ruthvik, P. Supraja, M. Navaneeth, K.U. Kumar, R.R. Kumar, K. Prakash, N. Raju, High-performance triboelectric nanogenerator using ZIF-67/PVDF hybrid film for energy harvesting, J. Mater. Sci. Mater. Electron. 34 (2023) 1–11, https://doi.org/10.1007/S10854-023-11644-8/METRICS.
[134] S.A. Behera, H.G. Kim, I.R. Jang, S. Hajra, S. Panda, N. Vittayakorn, H.J. Kim, P.G. R. Achary, Triboelectric nanogenerator for self-powered traffic monitoring, Mater. Sci. Eng., B 303 (2024) 117277, https://doi.org/10.1016/J.MSEB.2024.117277.
[135] K. Ruthvik, A. Babu, P. Supraja, M. Navaneeth, V. Mahesh, K. Uday Kumar, R. Rakesh Kumar, B. Manmada Rao, D. Haranath, K. Prakash, High-performance triboelectric nanogenerator based on 2D graphitic carbon nitride for self-powered electronic devices, Mater. Lett. 350 (2023) 134947, https://doi.org/10.1016/J.MATLET.2023.134947.
[136] S. Sardana, V. Sharma, K.G. Beepat, D.P. Sharma, A.K. Chawla, A. Mahajan, Flexible, humidity- and contamination-resistant superhydrophobic MXene-based electrospun triboelectric nanogenerators for distributed energy harvesting applications, Nanoscale 15 (2023) 19369–19380, https://doi.org/10.1039/D3NR04537D.
[137] D.P. Pabba, M. Satthiyaraju, A. Ramasdoss, P. Sakthivel, N. Chidhambaram, S. Dhanabalan, C.V. Abarzúa, M.J. Morel, R. Udayabhaskar, R.V. Mangalaraja, R. Aepuru, S.K. Kamaraj, P.K. Murugesan, A. Thirumurugan, MXene-Based nanocomposites for piezoelectric and triboelectric energy harvesting applications, Micromachines 14 (2023) 1273, https://doi.org/10.3390/MI14061273, 14 (2023) 1273.
[138] J.A. Ajani Lakmini Jayarathna, S. Hajra, S. Panda, E. Chamanehpour, I. Sulania, M. Singh Goyat, S.H. Hsu, H. Joon Kim, T. Treeratanaphitak, Y. Kumar Mishra, Exploring potential of MXenes in smart sensing and energy harvesting, Mater. Lett. 363 (2024) 136252, https://doi.org/10.1016/J.MATLET.2024.136252.
[139] Q. Jiang, C. Wu, Z. Wang, A.C. Wang, J.H. He, Z.L. Wang, H.N. Alshareef, MXene electrochemical microsupercapacitor integrated with triboelectric nanogenerator as a wearable self-charging power unit, Nano Energy 45 (2018) 266–272, https://doi.org/10.1016/J.NANOEN.2018.01.004.
[140] X. Luo, L. Zhu, Y.C. Wang, J. Li, J. Nie, Z.L. Wang, A flexible multifunctional triboelectric nanogenerator based on MXene/PVA hydrogel, Adv. Funct. Mater. 31 (2021) 2104928, https://doi.org/10.1002/ADFM.202104928.
[141] W. Qiao, L. Zhou, Z. Zhao, P. Yang, D. Liu, X. Liu, J. Liu, D. Liu, Z.L. Wang, J. Wang, MXene lubricated tribovoltaic nanogenerator with high Current output and long lifetime, Nano-Micro Lett. 15 (2023) 1–13, https://doi.org/10.1007/S40820-023-01198-Z/FIGURES/5.
[142] A. Mondal, M. Faraz, M. Dahiya, N. Khare, Double-Layer electronegative structure-based triboelectric nanogenerator for enhanced performance using combined effect of enhanced charge generation and improved charge trapping, ACS Appl. Mater. Interfaces (2024), https://doi.org/10.1021/ACSAMI.4C08964/SUPPL_FILE/AM4C08964_SI_001.PDF.
[143] M.A. Belal, H.H. Khalil, R.L. Mahajan, A.E. Rashed, S.N. Khattab, A.A. El-Moneim, Layered structure design of inkjet-printed graphene/Co3O4 for high-performance flexible microsupercapacitors, J. Energy Storage 101 (2024) 113900, https://doi.org/10.1016/J.EST.2024.113900.
[144] X. Yang, F. Wu, C. Xu, L. Yang, S. Yin, A flexible high-output triboelectric nanogenerator based on MXene/CNT/PEDOT hybrid film for self-powered wearable sensors, J. Alloys Compd. 928 (2022) 167137, https://doi.org/10.1016/J.JALLCOM.2022.167137.
[145] W. Cho, S. Kim, H. Lee, N. Han, H. Kim, M. Lee, T.H. Han, J.J. Wie, High-Performance yet sustainable triboelectric nanogenerator based on sulfur-rich polymer composite with MXene segregated structure, Adv. Mater. 36 (2024) 2404163, https://doi.org/10.1002/ADMA.202404163.
[146] O. Faruk, M.R. Islam, S.M.S. Rana, G.B. Pradhan, H.S. Kim, M. Asaduzzaman, T. Bhatta, J.Y. Park, V2CTX-MXene-functionalized fluoropolymer composite nanofibrous mat-based high-performance triboelectric nanogenerator for self-powered human activity and posture monitoring, Nano Energy 127 (2024) 109787, https://doi.org/10.1016/J.NANOEN.2024.109787.
[147] L. Kabir, K. Wijaya, W.C. Oh, Progressive MXene-based photocatalytic and electrocatalytic sustainable reduction of CO2 to chemicals: comprehensive review and future directions, Sustain. Energy Fuels 8 (2024) 2535–2569, https://doi.org/10.1039/D4SE00405A.
[148] Mxene-based Electrocatalysts for CO 2 Reduction: Advances, Challenges, and Perspectives - Materials Horizons (RSC Publishing) DOI:10.1039/D5MH00905G, (n.d.). https://pubs.rsc.org/en/content/articlehtml/2025/mh/d5mh00905g (accessed October 13, 2025).
[149] Q. Tang, T. Li, W. Tu, H. Wang, Y. Zhou, Z. Zou, Recent advances in diverse MXenes-Based structures for photocatalytic CO2 reduction into renewable hydrocarbon fuels, Adv. Funct. Mater. 34 (2024) 2311609, https://doi.org/10.1002/ADFM.202311609.
[150] A. Gulzar, A. Haleem, T.U. Rehman, M. Ullah, A. Shah, I. Ullah, Harnessing the power of MXenes: a comprehensive exploration of their photocatalytic potential in mitigating hazardous dyes and CO2 reduction, Discov. Mater. 4 (2024) 1–27, https://doi.org/10.1007/S43939-024-00081-X/TABLES/3.
[151] D.E. Lee, V. Devthade, B.M. Abraham, W.K. Jo, S. Tonda, An S-scheme heterointerface-engineered high-performance ternary NiAl-LDH@TiO2/Ti3C2

MXene photocatalytic system for solar-powered CO2 reduction to produce energy-rich fuels, Chem. Eng. J. 480 (2024) 148227, https://doi.org/10.1016/J.CEJ.2023.148227.
[152] F.M. Pesci, G. Wang, D.R. Klug, Y. Li, A.J. Cowan, Efficient suppression of electron–hole recombination in oxygen-deficient hydrogen-treated TiO2 nanowires for photoelectrochemical water splitting, J. Phys. Chem. C 117 (2013) 25837–25844, https://doi.org/10.1021/JP4099914.
[153] S. Jin, Z. Shi, H. Jing, L. Wang, Q. Hu, D. Chen, N. Li, A. Zhou, Mo2C-MXene/CdS heterostructures as visible-light photocatalysts with an ultrahigh hydrogen production rate, ACS Appl. Energy Mater. 4 (2021) 12754–12766, https://doi.org/10.1021/ACSAEM.1C02456/SUPPL_FILE/AE1C02456_SI_002.MOV.
[154] Y. Wang, C. Dong, D. Hu, R. Tokarz-Sobieraj, D. Rutkowska-Zbik, K. Ben Tayeb, A. Addad, V. Butenko, E. de la Torre Miranda, M.N. Tran, P. Simon, O. Safonova, V. Briois, V.V. Ordomsky, A.Y. Khodakov, In-situ exploration of divergent methane coupling pathways in dry and aqueous environments on silver and palladium heteropolyacid-titania photocatalysts, Appl. Catal. B Environ. Energy 358 (2024) 124400, https://doi.org/10.1016/J.APCATB.2024.124400.
[155] H.H. Cao, Z.H. He, P.P. Guo, Y. Tian, X. Wang, K. Wang, W. Wang, H. Wang, Y. Yang, Z.T. Liu, N-doped Ti3C2Tx MXene-regulated metal-oxide facilitates the efficient electrocatalytic CO2 reduction to CO, ChemCatChem 17 (2025) e202401133, https://doi.org/10.1002/CCTC.202401133.
[156] Y. Liu, Y. Xu, X. Pang, B. Zhang, Y. Gao, Z. Hu, Y. Miao, W. Tian, H. Jing, The cooperative p-n heterojunction and Schottky junction in Cu-coated Cu2O/TiO2/Ti3C2 for efficiently photoelectrocatalytic CO2 reduction to ethanol, J. Alloys Compd. 1017 (2025) 179012, https://doi.org/10.1016/J.JALLCOM.2025.179012.
[157] Z. Otgonbayar, W.C. Oh, Comprehensive-designed graphene-based quaternary nanocomposite and its synergistic effect towards photoelectrocatalytic CO2 reduction under different electrolytes, Fuel 364 (2024) 131161, https://doi.org/10.1016/J.FUEL.2024.131161.
[158] S. Çetinkaya, L. Özcan, L. Palmisano, S. Yurdakal, Partial photoelectrocatalytic oxidation of 3-Methylpiridine in green conditions by Nanotube/Nanowire Ti/TiO2 plates prepared in aqueous, glycerol, or ethylene glycol medium, ChemCatChem 16 (2024) e202400755, https://doi.org/10.1002/CCTC.202400755.
[159] J. Yu, X. Hao, L. Mu, W. Shi, G. She, Photoelectrocatalytic utilization of CO2: a big show of Si-based photoelectrodes, Chem. Eur J. 30 (2024) e202303552, https://doi.org/10.1002/CHEM.202303552.
[160] Q.T.H. Ta, M.H. Tran, T.M.H. Nguyen, P.K.T. Nguyen, D.H. Nguyen, Engineering heterojunction noble metal (NM)@ZnO catalyst for improved CH4 photocatalytic oxidation, Inorg. Chem. Commun. 170 (2024) 113345, https://doi.org/10.1016/J.INOCHE.2024.113345.
[161] Q.T.H. Ta, L.M. Nguyen, N.H. Nguyen, P.K.T. Nguyen, D.H. Nguyen, Photocatalytic methane oxidation over a TiO2/SiNWs p–n junction catalyst at room temperature, Beilstein J. Nanotechnol. 15 (92 15) (2024) 1132–1141, https://doi.org/10.3762/BJNANO.15.92.
[162] Y. Xu, F. Wang, S. Lei, Y. Wei, D. Zhao, Y. Gao, X. Ma, S. Li, S. Chang, M. Wang, H. Jing, In situ grown two-dimensional TiO2/Ti3CN MXene heterojunction rich in Ti3+ species for highly efficient photoelectrocatalytic CO2 reduction, Chem. Eng. J. 452 (2023) 139392, https://doi.org/10.1016/J.CEJ.2022.139392.
[163] P. Chen, Y. Zhang, Y. Zhou, F. Dong, Photoelectrocatalytic carbon dioxide reduction: fundamental, advances and challenges, Nano Materials Science 3 (2021) 344–367, https://doi.org/10.1016/J.NANOMS.2021.05.003.
[164] K.M.R. Karim, M. Tarek, S.M. Sarkar, R. Mouras, H.R. Ong, H. Abdullah, C. K. Cheng, M.M.R. Khan, Photoelectrocatalytic reduction of CO2 to methanol over CuFe2O4@PANI photocathode, Int. J. Hydrogen Energy 46 (2021) 24709–24720, https://doi.org/10.1016/J.IJHYDENE.2020.02.195.
[165] Z. Pan, E. Han, J. Zheng, J. Lu, X. Wang, Y. Yin, G.I.N. Waterhouse, X. Wang, P. Li, Highly efficient photoelectrocatalytic reduction of CO2 to methanol by a p–n heterojunction CeO2/CuO/Cu catalyst, Nano-Micro Lett. 12 (2020) 1–13, https://doi.org/10.1007/S40820-019-0354-1/FIGURES/5.
[166] Z. Zhang, X. Ding, X. Yang, W. Tu, L. Wang, Z. Zou, Shedding light on CO2: catalytic synthesis of solar methanol, EcoMat 3 (2021) e12078, https://doi.org/10.1002/EOM2.12078.
[167] B. Shang, F. Zhao, S. Suo, Y. Gao, C. Sheehan, S. Jeon, J. Li, C.L. Rooney, O. Leitner, L. Xiao, H. Fan, M. Elimelech, L. Wang, G.J. Meyer, E.A. Stach, T. E. Mallouk, T. Lian, H. Wang, Tailoring interfaces for enhanced methanol production from photoelectrochemical CO2 reduction, J. Am. Chem. Soc. 146 (2024) 2267–2274, https://doi.org/10.1021/JACS.3C13540/SUPPL_FILE/JA3C13540_SI_001.MP4.
[168] C. Huazhen, Y. Yihang, F. Wenyu, Z. Huibin, Crafting CuxS-ReS2 semiconductor with enhanced adsorption capacity to facilitate photoelectrocatalytic ethanol production from CO2, Int. J. Hydrogen Energy 69 (2024) 68–78, https://doi.org/10.1016/J.IJHYDENE.2024.04.227.
[169] N. Nandal, P.K. Prajapati, B.M. Abraham, S.L. Jain, CO2 to ethanol: a selective photoelectrochemical conversion using a ternary composite consisting of graphene oxide/copper oxide and a copper-based metal-organic framework, Electrochim. Acta 404 (2022) 139612, https://doi.org/10.1016/J.ELECTACTA.2021.139612.
[170] M. Wang, M. Langer, R. Altieri, M. Crisci, S. Osella, T. Gatti, Two-Dimensional layered heterojunctions for photoelectrocatalysis, ACS Nano 18 (2024) 9245–9284, https://doi.org/10.1021/ACSNANO.3C12274.
[171] S. Bagheri, A. Lipatov, N.S. Vorobeva, A. Sinitskii, Interlayer incorporation of A-Elements into MXenes via selective etching of A′ from Mn+1A′1-xA″xCn MAX phases, ACS Nano 17 (2023) 18747–18757, https://doi.org/10.1021/ACSNANO.3C02198/ASSET/IMAGES/LARGE/NN3C02198_0006.JPEG.
[172] M. Anayee, R. (John, Wang, M. Downes, S. Ippolito, Y. Gogotsi, Layer-by-layer mechanism of the MAX phase to MXene transformation, Matter 0 (2025), https://doi.org/10.1016/J.MATT.2025.102092/ATTACHMENT/313A7CD5-A3A3-41EF-AF8E-F950613483C2/MMC3.PDF.
[173] M.L. Matias, C. Pereira, H.V. Almeida, S. Jana, S. Panigrahi, U.D. Menda, D. Nunes, E. Fortunato, R. Martins, S. Nandy, 3D printed MXene architectures for a plethora of smart applications, Mater Today Adv 23 (2024) 100512, https://doi.org/10.1016/J.MTADV.2024.100512.
[174] S.P. Sreenilayam, I. Ul Ahad, V. Nicolosi, D. Brabazon, MXene materials based printed flexible devices for healthcare, biomedical and energy storage applications, Mater. Today 43 (2021) 99–131, https://doi.org/10.1016/J.MATTOD.2020.10.025.
[175] Z. Wu, S. Liu, Z. Hao, X. Liu, MXene contact engineering for printed electronics, Adv. Sci. 10 (2023) 2207174, https://doi.org/10.1002/ADVS.202207174;WGROUP:STRING:PUBLICATION.
[176] M.A. Belal, R. Yousry, G. Taulo, A.A. AbdelHamid, A.E. Rashed, A.A. El-Moneim, Layer-by-Layer inkjet-printed manganese oxide nanosheets on graphene for high-performance flexible supercapacitors, ACS Appl. Mater. Interfaces 15 (2023) 53632–53643, https://doi.org/10.1021/ACSAMI.3C07339/SUPPL_FILE/AM3C07339_SI_001.PDF.
[177] M.A. Belal, S. Hajra, S. Panda, K.R. Kaja, M.M.M. Abdo, A. Abd El-Moneim, D. Janas, Y.K. Mishra, H.J. Kim, Advances in gas sensors using screen printing, J Mater Chem A Mater 13 (2025) 5447–5497, https://doi.org/10.1039/D4TA06632D.
[178] G.T. Taulo, A.E. Moharm, M.A. Belal, N.M. Shaalan, M.M. Ayad, G.G. Mohamed, A.A. El-Moneim, Impact of NS co-doped rGO on the CO gas sensing performance of inkjet-printed SnO2 nanoparticles, Sensor. Actuator. B Chem. 443 (2025) 138186, https://doi.org/10.1016/J.SNB.2025.138186.
[179] A.M. Bayoumy, A. Hessein, M. Ahmed Belal, M. Ezzat, M.A. Ibrahim, A. Osman, A. Abd El-Moneim, Microdrop InkJet printed supercapacitors of graphene/graphene oxide ink for flexible electronics, J. Power Sources 617 (2024) 235145, https://doi.org/10.1016/J.JPOWSOUR.2024.235145.
[180] M.A. Belal, R. Yousry, G. Taulo, A.A. AbdelHamid, A.E. Rashed, A.A. El-Moneim, Layer-by-Layer inkjet-printed manganese oxide nanosheets on graphene for high-performance flexible supercapacitors, ACS Appl. Mater. Interfaces 15 (2023) 53632–53643, https://doi.org/10.1021/ACSAMI.3C07339.
[181] S. Nouseen, M. Pumera, S. Nouseen, M. Pumera, MXene 3D/4D printing: ink formulation and electrochemical energy storage applications, Adv. Funct. Mater. 35 (2025) 2421987, https://doi.org/10.1002/ADFM.202421987.
[182] Z. Li, Q. He, H. Chen, Y. Chen, C. Zeng, T. Xu, S. Deng, C. Zhang, Multifunctional MXene inks for printed electrochemical energy storage devices, Energy Mater 5 (2025) 500005, https://doi.org/10.20517/ENERGYMATER.2024.31, 5 (2025) N/A-N/A.
[183] F.R. Kouchi, T.V. Varghese, H. Burgoyne, N.E. Mansoor, M.-L. Seol, N. Mckibben, S. Nirantar, K. Chinnathambi, J. Eixenberger, O. Maryon, C.E. Shuck, Y. Gogotsi, J.E. Koehne, D. Estrada, F.R. Kouchi, T. V Varghese, H. Burgoyne, N.E. Mansoor, N. Mckibben, S. Nirantar, K. Chinnathambi, O. Maryon, D. Estrada, M.-L. Seol, J. E. Koehne, StableTi3C2Tx MXene ink formulation and high-resolution aerosol jet printing for high-performance MXene supercapacitors, Small Methods (2025) 2500499, https://doi.org/10.1002/SMTD.202500499.
[184] M.A. Belal, S. Hajra, S. Panda, K.R. Kaja, K.J. Park, H.J. Kim, Spray-printed ZnO thin film for high-sensitivity NO2 gas sensing, Micro and Nano Systems Letters 13 (2025) 1–11, https://doi.org/10.1186/S40486-025-00230-8/FIGURES/6.
[185] M.A. Belal, S. Hajra, S. Panda, K.R. Kaja, A.A. El-Moneim, P.G.R. Achary, H. J. Kim, Mechanochemically synthesized ZIF-8@ZnO composite-based NO2 gas detection, New J. Chem. (2025), https://doi.org/10.1039/D5NJ02514A.
[186] H. Huang, W. Yang, MXene-Based Micro-Supercapacitors: ink rheology, microelectrode design and integrated System, ACS Nano 18 (2024) 4651–4682, https://doi.org/10.1021/ACSNANO.3C10246.
[187] C. John Zhang, L. McKeon, M.P. Kremer, S.H. Park, O. Ronan, A. Seral-Ascaso, S. Barwich, C. Coileáin, N. McEvoy, H.C. Nerl, B. Anasori, J.N. Coleman, Y. Gogotsi, V. Nicolosi, Additive-free MXene inks and direct printing of micro-supercapacitors, Nat. Commun. 10 (2019) 1–9, https://doi.org/10.1038/S41467-019-09398-1. TECHMETA.
[188] S. Abdolhosseinzadeh, R. Schneider, A. Verma, J. Heier, F. Nüesch, C. Zhang, Turning trash into treasure: additive free MXene sediment inks for screen-printed micro-supercapacitors, Adv. Mater. 32 (2020) 2000716, https://doi.org/10.1002/ADMA.202000716.
[189] A. Bigham, A. Zarepour, A. Khosravi, S. Iravani, A. Zarrabi, 3D and 4D printing of MXene-based composites: from fundamentals to emerging applications, Mater. Horiz. 11 (2024) 6257–6288, https://doi.org/10.1039/D4MH01056F.
[190] H.T.A. Awan, M.A.A.M. Abdah, M. Mehar, R. Walvekar, V. Chaudhary, M. Khalid, A. Khosla, MXene-polymer hybrid composites for advanced energy storage: insights into supercapacitors and batteries, J. Energy Storage 95 (2024) 112449, https://doi.org/10.1016/J.EST.2024.112449.
[191] C. Zhang, L. McKeon, M.P. Kremer, S.H. Park, O. Ronan, A. Seral-Ascaso, S. Barwich, C.O. Coileáin, N. McEvoy, H.C. Nerl, B. Anasori, J.N. Coleman, Y. Gogotsi, V. Nicolosia, Additive-free MXene inks and direct printing of micro-supercapacitors, MXenes: From Discovery to Applications of Two-Dimensional Metal Carbides and Nitrides (2023) 463–485, https://doi.org/10.1201/9781003306511-23/ADDITIVE-FREE-MXENE-INKS-DIRECT-PRINTING-MICRO-SUPERCAPACITORS-CHUANFANG-JOHN-ZHANG-LORCAN-MCKEON-MATTHIAS-KREMER-SANG-HOON-PARK-OSKAR-RONAN-ANDR.
[192] P. Viviani, E. Gibertini, V. Montanelli, L. Magagnin, Zinc plating on inkjet-printed Ti3C2Tx MXene: effect of electrolyte and PEG additive, Appl. Sci. 14 (2024) 682, https://doi.org/10.3390/APP14020682/S1.

[193] P. Viviani, E. Gibertini, P. Fontana, F. Lissandrello, Y. Gogotsi, L. Magagnin, Flexible inkjet-printed lithium-ion batteries with Ti3C2Tx current collector, J. Power Sources 601 (2024) 234287, https://doi.org/10.1016/J.JPOWSOUR.2024.234287.

[194] Y. Zhu, Q. Zhang, J. Ma, P. Das, L. Zhang, H. Liu, S. Wang, H. Li, Z.S. Wu, Three-dimensional (3D)-printed MXene high-voltage aqueous micro-supercapacitors with ultrahigh areal energy density and low-temperature tolerance, Carbon Energy 6 (2024) e481, https://doi.org/10.1002/CEY2.481;PAGEGROUP:STRING:PUBLICATION.

[195] A.M. Bayoumy, A. Hessein, M. Ahmed Belal, M. Ezzat, M.A. Ibrahim, A. Osman, A. Abd El-Moneim, Microdrop InkJet printed supercapacitors of graphene/graphene oxide ink for flexible electronics, J. Power Sources 617 (2024) 235145, https://doi.org/10.1016/J.JPOWSOUR.2024.235145.

[196] H. Tetik, J. Orangi, G. Yang, K. Zhao, S. Bin Mujib, G. Singh, M. Beidaghi, D. Lin, 3D printed MXene aerogels with truly 3D macrostructure and highly engineered microstructure for enhanced electrical and electrochemical performance, Adv. Mater. 34 (2022) 2104980, https://doi.org/10.1002/ADMA.202104980.

[197] Y. Wang, Y. Yuan, H.Y. Geng, W. Yang, X. Chen, Boosting ion diffusion kinetics of MXene inks with water-in-salt electrolyte for screen-printed micro-supercapacitors, Adv. Funct. Mater. 34 (2024) 2400887, https://doi.org/10.1002/ADFM.202400887.

[198] S. Zheng, J. Ma, K. Fang, S. Li, J. Qin, Y. Li, J. Wang, L. Zhang, F. Zhou, F. Liu, K. Wang, Z.S. Wu, High-Voltage potassium ion micro-supercapacitors with extraordinary volumetric energy density for wearable pressure sensor System, Adv. Energy Mater. 11 (2021) 2003835, https://doi.org/10.1002/AENM.202003835.

[199] G. Zhou, X. Liu, C. Liu, Z. Li, C. Liu, X. Shi, Z. Li, C. Mei, M.C. Li, 3D printed MXene-based films and cellulose nanofiber reinforced hydrogel electrolyte to enable high-performance flexible supercapacitors, J Mater Chem A Mater 12 (2024) 3734–3744, https://doi.org/10.1039/D3TA06925G.

[200] Q. Zhou, C. Zhu, H. Xue, L. Jiang, J. Wu, Flexible, wearable wireless-charging power System incorporating piezo-ultrasonic arrays and MXene-Based solid-state supercapacitors, ACS Appl. Mater. Interfaces 16 (2024) 35268–35278, https://doi.org/10.1021/ACSAMI.4C03143/SUPPL_FILE/AM4C03143_SI_001.PDF.

[201] P. Sun, J. Liu, Q. Liu, J. Yu, R. Chen, J. Zhu, G. Sun, Y. Li, D. Song, J. Wang, Stable 3D porous N-MXene/NiCo2S4 network with Ni–O atomic bridging for printed hybrid micro-supercapacitors, Chem. Eng. J. 493 (2024) 152731, https://doi.org/10.1016/J.CEJ.2024.152731.

[202] N. Dey, A. Yadav, S.K. Ray, P.K. Guha, Printed MXene-NiSe asymmetric micro-supercapacitors for flexible energy storage devices, J. Energy Storage 98 (2024) 112831, https://doi.org/10.1016/J.EST.2024.112831.

[203] J. Ma, S. Zheng, Y. Cao, Y. Zhu, P. Das, H. Wang, Y. Liu, J. Wang, L. Chi, S. Liu, Z. S. Wu, Aqueous MXene/PH1000 hybrid inks for inkjet-printing micro-supercapacitors with unprecedented volumetric capacitance and modular self-powered microelectronics, Adv. Energy Mater. 11 (2021) 2100746, https://doi.org/10.1002/AENM.202100746.

[204] S. Mappoli, K. Ghosh, M. Pumera, MXene and polyaniline coated 3D-printed carbon electrode for asymmetric supercapacitor, Virtual Phys. Prototyp. 19 (2024), https://doi.org/10.1080/17452759.2024.2361139.

[205] S. Ahmad, M. Imran, F. Hussain, U. Rasheed, A.M. Tighezza, R.M.A. Khalil, M. N. Ashiq, M. Irfan, M.F. Ehsan, Metal layer intercalation with Mxene to enhance the performance of supercapacitor: using DFT approach, J. Energy Storage 113 (2025) 115728, https://doi.org/10.1016/J.EST.2025.115728.

[206] M. Adeel, H.S. Lee, K. Asif, S. Smith, H. Kurt, F. Rizzolio, S. Daniele, F. Güder, Micro-Supercapacitors for self-powered biosensors, Small Science 4 (2024) 2400096, https://doi.org/10.1002/SMSC.202400096.

[207] G. Saeed, T. Kang, J.S. Byun, D. Min, J.S. Kim, S.V. Sadavar, H.S. Park, Two-dimensional (2D) materials for 3D printed micro-supercapacitors and micro-batteries, Energy Mater 4 (2024) 400023, https://doi.org/10.20517/ENERGYMATER.2023.81, 4 (2024) N/A-N/A.

[208] J. Ma, S. Zheng, Y. Fu, X. Wang, J. Qin, Z.S. Wu, The status and challenging perspectives of 3D-printed micro-batteries, Chem. Sci. 15 (2024) 5451–5481, https://doi.org/10.1039/D3SC06999K.

[209] L. Feng, S. Zhou, H. Cui, R.A. Soomro, P. Zhang, B. Xu, Multi-functional MXene binder enables ultra-stable and high-capacity Li4Ti5O12 anode for lithium ion batteries, Energy Storage Mater. 75 (2025) 104079, https://doi.org/10.1016/J.ENSM.2025.104079.

[210] W. Myint, K. Lolupiman, C. Yang, P. Woottapanit, W. Limphirat, P. Kidkhunthod, M. Muzakir, M. Karnan, X. Zhang, J. Qin, Exploring the electrochemical superiority of V2O5/TiO2@Ti3C2-MXene hybrid nanostructures for enhanced lithium-ion battery performance, ACS Appl. Mater. Interfaces 16 (2024) 53764–53774, https://doi.org/10.1021/ACSAMI.4C10656/ASSET/IMAGES/LARGE/AM4C10656_0008.JPEG.

[211] G. Zhu, H. Zhang, J. Lu, Y. Hou, P. Liu, S. Dong, H. Pang, Y. Zhang, 3D printing of MXene-Enhanced ferroelectric polymer for ultrastable zinc anodes, Adv. Funct. Mater. 34 (2024) 2305550, https://doi.org/10.1002/ADFM.202305550.

[212] H. Lu, J. Hu, K. Zhang, J. Zhao, S. Deng, Y. Li, B. Xu, H. Pang, Microfluidic-Assisted 3D printing zinc powder anode with 2D Conductive MOF/MXene heterostructures for high-stable Zinc−Organic battery, Adv. Mater. 36 (2024) 2309753, https://doi.org/10.1002/ADMA.202309753.

[213] C. Cao, S. Tang, X. Wu, H. Huang, S. Liu, H. Li, C. Cao, S. Tang, X. Wu, H. Huang, S. Liu, H. Li, Sustainable MXene/Conductive cellulose heteroinks for 3D printed high areal energy density micro-supercapacitors and self-powered integrated systems, Adv. Sci. (2025) e11439, https://doi.org/10.1002/ADVS.202511439.

[214] Y. Zhou, J. Li, H. Fu, N. Li, S. Chai, T. Duan, L. Xu, Z.J. Wang, J. Xu, Additive-Free Ti3C2Tx MXene/Carbon nanotube aqueous inks enable energy density enriched 3D-Printed flexible micro-supercapacitors for modular self-powered systems, Carbon Energy 7 (2025) e698, https://doi.org/10.1002/CEY2.698.

[215] S. Gu, G. Du, Y. Su, Y. Zhang, Y. Zhang, L. Li, H. Pang, H. Zhou, Architectural design and optimization of internal structures in 3D printed electrodes for superior supercapacitor performance, J. Colloid Interface Sci. 677 (2025) 21–29, https://doi.org/10.1016/J.JCIS.2024.08.053.

[216] Z. Ji, Y. Feng, L. Liu, W. Zheng, M. Wu, Y. Li, Z. Sun, G. Ying, Inkjet-printed flexible V2CTx film electrodes with excellent photoelectric properties and high capacities for energy storage device, J. Colloid Interface Sci. 678 (2025) 200–209, https://doi.org/10.1016/J.JCIS.2024.09.001.

[217] N. Sharma, S. Kale, N. Thomas, S. Kale, D. Ray, P. Swaminathan, Titanium carbide MXene and silver nanowire composite ink for transparent flexible Printed Micro-Supercapacitors, Batter Supercaps (2025) 2500319, https://doi.org/10.1002/BATT.202500319.

[218] X. Du, X. Zhang, Q. Li, H. Ren, W. Tang, Y. Wei, J. Liang, W. Wu, Achieving long-life CoNi-PBA/MXene composite cathode for printed flexible supercapacitor, Mater. Today Energy 53 (2025) 102046, https://doi.org/10.1016/J.MTENER.2025.102046.

[219] B. Ding, L. Yao, J. Tang, C. Li, X. Zheng, Screen-printed MXene-based all-solid-state textile supercapacitors, Mater. Today Commun. 38 (2024) 108170, https://doi.org/10.1016/J.MTCOMM.2024.108170.

[220] N. Dey, A. Yadav, S.K. Ray, P.K. Guha, Printed MXene-NiSe asymmetric micro-supercapacitors for flexible energy storage devices, J. Energy Storage 98 (2024) 112831, https://doi.org/10.1016/J.EST.2024.112831.

[221] B. Balan, S. Ramasamy, S.P. Rajendra, M.S. AlSalhi, S. Angaiah, Advanced (Cu, Co)Se2 nanocubes and Ti-MXene based screen printed electrodes for high performance flexible microsupercapacitors, Adv. Funct. Mater. 34 (2024) 2408639, https://doi.org/10.1002/ADFM.202408639.